

# High Order Modified Weighted Compact Scheme for High Speed Flow

Chaoqun Liu  
Peng Xie  
Maria L. Oliveira

Technical Report 2007-15

<http://www.uta.edu/math/preprint/>

# High Order Modified Weighted Compact Scheme for High Speed Flow

(TECHNICAL REPORT FOR THE 2007 VA SUMMER PROGRAM)

CHAOQUN LIU, PENG XIE & MARIA L OLIVEIRA  
UNIVERSITY OF TEXAS AT ARLINGTON, ARLINGTON, TX 76019  
CLIU@UTA.EDU

## ABSTRACT

The critical problem of CFD is perhaps an accurate approximation of derivatives for a given discrete data set. Based on our previous work on the weighted compact scheme (WCS), a modified weighted compact scheme (MWCS) has been developed. Similar to WENO, three high order candidates, left, right, and central, are constructed by Hermite polynomials. According to the smoothness, three weights are derived and assigned to each candidate. The weights will lead the scheme to be bias when approaching the shock or other discontinuities but quickly becomes central, compact, and of high order just off the shock. Therefore, the new scheme can get a sharp shock without oscillation, but keep central, compact and of high resolution in the smooth area. This feature is particularly important to numerical simulation of the shock-boundary layer interaction, where both shock and small eddies are important. The new scheme has three compact candidate stencils,  $E_0, E_1, E_2$ , with three weights  $\omega_0, \omega_1, \omega_2$ . Candidate stencils  $E_0, E_1, E_2$  have third order, fourth order, and third order of accuracy respectively. Picking  $\omega_0 = \frac{1}{18}, \omega_1 = \frac{8}{9}, \omega_2 = \frac{1}{18}$ , MWCS has sixth order of accuracy in the smooth area. For near shock grid points,  $\omega_0 = 1, \omega_1 = 0, \omega_2 = 0$ , MWCS still has fourth order of accuracy. Comparing with 5<sup>th</sup> order WENO which has 5<sup>th</sup> order in the smooth area and third order near the shock, MWCS is super with smaller stencils and higher order of accuracy. The necessary dissipation is provided by weights and some high order bias up-winding scheme. The new scheme has been successfully applied for 1-D shock tube and shock-entropy interaction and 2-D incident shock. The new scheme has obtained sharper shock, no deformation for expansion wave, and much higher resolution than 5<sup>th</sup> order WENO for small length scales. A first version of a black-box type subroutine with MWCS scheme has been developed and given to AFRL collaborators. The subroutine can give a high order derivative for any discrete data sets, no matter they are smooth, highly oscillatory, or no-differentiable. The scheme is currently applied for shock-boundary layer interaction with double cones for validation. A variety of cases including shock-boundary interaction with incident shock, double angles and double-cones is being tested.

The preliminary numerical solution is encouraging while the numerical simulation with double angles and double cones are still running. The new effort will also focus on new versions of the black-box type subroutines. The first version requires explicit boundary values. The second version will be able to treat variety of boundary conditions implicitly and keep high order for the

boundary points. The third and fourth version will include fast computation and self flux splitting.

## **1. Introduction**

### **1.1 A short overview on shock capturing schemes**

The flow field is in general governed by the Navier-Stokes system which is a system of time dependent partial differential equations. However, for external flow, the viscosity is important largely only in the boundary layers. The main flow can still be considered as inviscid and the governing system can be dominated by the time dependent Euler equations which are hyperbolic. The difficult problem with numerical solution is the shock capturing which can be considered as a discontinuity or mathematical singularity (no classical unique solution and no bounded derivatives). In the shock area, continuity and differentiability of the governing Euler equations are lost and only the weak solution in an integration form can be obtained. The shock can be developed in some cases because the Euler equation is non-linear and hyperbolic. On the other hand, the governing Navier-Stokes system presents parabolic type behavior in and is therefore dominated by viscosity or second order derivatives. One expects that the equation should be solved by high order central difference scheme, high order compact scheme is preferable, to get high order accuracy and high resolution. High order of accuracy is critical in resolving small length scale in flow transition and turbulence process. However, for the hyperbolic system, the analysis already shows the existence of characteristic lines and Riemann invariants. Apparently, the upwind finite difference scheme coincides with the physics for a hyperbolic system. History has shown the great success of upwind technologies. We should consider not only the eigenvalues and eigenvectors of the Jacobian system, but also non-linearity including the Rankine-Hugoniot shock relations. From the point of view of shocks, it makes no sense to use high order compact scheme for shock capturing which use all grid points on one grid line to calculate the derivative by solving a tri-diagonal or penta-diagonal linear system when shock does not have finite derivatives and downstream quantities cannot cross shock to affect the upstream points. From the point of view of the above statement, upwind scheme is appropriate for the hyperbolic system. Many upwind or bias upwind schemes have achieved great success in capturing the shocks sharply, such as Godunov (1959), Roe (1981), MUSCL (Van Leer, 1979), TVD (Harten, 1983), ENO (Harten et al, 1987; Shu et al, 1988, 1989) and WENO (Liu et al, 1994; Jiang et al, 1996). Roe's scheme may be better in capturing the shock sharply because it satisfies the Rankine-Hugoniot relation. Of course, Roe's method can also be considered as a method for flux difference splitting and any high order method such as ENO and WENO can use Roe's method as a splitting method. However, all these shock-capturing schemes are based on upwind or bias upwind technology, which is nice for hyperbolic system, but is not favorable to the N-S system which presents parabolic equation behavior. The small length scale is very important in the flow transition and turbulence process and thus very sensitive to any artificial numerical dissipation. High order compact scheme (Lele, 1992; Visble, 2002) is more appropriate for simulation of flow transition and turbulence because it is central and non-dissipative with high order accuracy and high resolution.

Unfortunately, the shock-boundary layer interaction, which is important to high speed flow, is a mixed type problem which has shock (discontinuity), boundary layer (viscosity), separation,

transition, expansion fans, fully developed turbulence, and reattachment. In order to capture the shock and keep high order accuracy and high resolution in the smooth area, we have developed the so called weighted compact scheme (WCS, Jiang et al, 2001) which works very well for 1-D convection equation, Burger's equation, but not so good for Euler's equation with shocks. Visible wiggles have been found near the shock. In the case of shock-boundary layer interaction, there are elliptic areas (separation, transition, turbulence) and hyperbolic areas (main flow, shocks, expansion fans), which makes the accurate numerical simulation extremely difficult if not impossible. We have to divide the computational domain to several parts: the elliptic, hyperbolic, and mixed. The division or detection can be performed by switch function automatically such as shock detector which simply sets  $\Omega = 1$  for the shock area and  $\Omega = 0$  for the rest. The switch function may give the best results for shock-boundary layer interaction, but it will have too many logical statements in the code which may slow down the computation. The switch function could also be case-related and very difficult to adjust. It would also slow down the convergence for steady problems. The use of "weights" will be naturally considered as a good candidate that succeeded for many schemes, WENO is a good example and our Weighted Compact Scheme is another example.

Traditional finite difference schemes use the idea of Lagrange interpolation. To obtain  $n$ th order of accuracy, a stencil covering  $n+1$  grid points is needed. In other words, the derivative at a certain grid point depends upon the function values at these  $n+1$  grid points and only these grid points. In contrast, standard compact schemes (Lele, 1992; Visbal, 2002) use the idea of Hermitian interpolation. By using derivatives as well as function values, a compact scheme achieves high order of accuracy without increasing the width of stencils. As discussed in Lele's paper, a compact scheme has not only high order of accuracy, but also high resolution. Fourier analysis indicates that, with the same order of accuracy, a compact scheme has better spectral resolution than a traditional, explicit finite difference scheme. For this reason, compact schemes are favorable in the simulation of turbulent flows where small-length-scale structures are important.

Due to the usage of derivatives, compact schemes usually give us a tri-diagonal or penta-diagonal system. Although the tri-diagonal matrix is sparse, the inverse of a tri-diagonal matrix is dense, which means the derivative at a certain grid point depends upon all the grid points along a grid line. The success of compact schemes indicates that the global dependency is very important for high resolution. However, the global dependency is good for resolution but not so applicable for shock capturing.

The basic idea proposed in ENO (Harten et al, 1987) and WENO (Jiang et al, 1996) schemes is to avoid the stencil containing a shock. ENO chooses the smoothest stencil from several candidates to calculate the derivatives. WENO controls the contributions of different stencils according to their smoothness. In this way, the derivative at a certain grid point, especially one near the shock, is dependent on a very limited number of grid points. The local dependency here is favorable for shock capturing and helps obtaining the non-oscillatory property. The success of ENO and WENO schemes indicates that the local dependency is critical for shock capturing.

The Weighted Compact Scheme (WCS) we developed (Jiang et al, 2001) is constructed by introducing the idea of WENO scheme to the standard compact schemes which uses weights for

several candidates. The building block for each candidate is a Lagrange polynomial in WENO, but is Hermite in WCS. Therefore WCS achieves a higher accuracy with same stencil width. In shock regions, WCS controls the contributions of different candidate stencils to minimize the influence of the candidate which contains a shock. In smooth regions where shocks are not present, WCS recovers to the standard compact scheme to achieve high accuracy and resolution. The numerical tests indicate that original WCS works fine in some cases such as convection equation and Burger's equation, but not very well for Euler equation. As mentioned above, the usage of derivatives by compact schemes results in the global dependency.

In order to overcome the drawback of the WCS scheme, we need to achieve local dependency in shock regions and recover the global dependency in smooth regions. This fundamental idea will naturally lead to a combination of local dependent scheme, e.g. WENO and global dependent weighted compact schemes which we call "Modified Weighted Compact Scheme" (MWCS). The mixing and weights are designed in following ways: the new scheme automatically becomes bias when approaching the shock, but rapidly recovers to be central, compact, with high order of accuracy and high resolution. This kind of scheme has been developed and preliminary computation results are very promising. The new scheme needs to be optimized and validated for 2-D and 3-D cases.

## 1.2 Importance of high order scheme to DNS/LES

It should be pointed out that the order of accuracy of the finite difference scheme is absolutely not a trivial issue to CFD, especially to DNS and LES. There is a significant difference in requirements of grid size by DNS/LES between low order schemes and high order schemes. Let us take a look at the local truncation error for 1-D problem. If one uses a second order scheme with a mesh size of  $\Delta x_2$  and wants to have same truncation error using a sixth order scheme with a mesh size of  $\Delta x_6$ , one should have:

$$C_2(\Delta x_2)^2 = C_6(\Delta x_6)^6 \quad (1.1)$$

Assume  $C_2 \approx C_6$  and  $\Delta x_6 = 0.01$  (100 grid points in a normalized domain), we will get

$$\begin{aligned} (\Delta x_2)^2 &= (10^{-2})^6 \\ \Delta x_2 &= 10^{-6} \end{aligned} \quad (1.2)$$

In other words, the second order scheme needs one million of grid points to beat the sixth order scheme with 100 grid points for same order of accuracy. This advantage of high order scheme will become more significant when one uses DNS for 3-D problems. We do not want to use one million of grids in each direction for DNS, but prefer to use 100 grid points. Therefore high order scheme must be used. Of course, the global accuracy is also influenced by factors other than the local truncation errors, and the advantage of the sixth order scheme does not typically show a magnitude of 10 thousand times improvement over the second order scheme. However, it is now widely recognized that high order finite schemes are strongly encouraged to be used for DNS and LES which have much higher accuracy and higher resolution than low order schemes.

## 1.3 Comments on low order LES with low order subgrid models

Most LES computations require use of a subgrid model trying to get the unresolved scales back, which could be mathematically considered as truncation errors. Let us take a look at the famous Smagorinsky model:

$$\begin{aligned}\tau_{ij} &= -\nu_t S_{ij} \text{ and} \\ \nu_t &= (C_s \Delta)^2 |S|\end{aligned}\tag{1.3}$$

Where  $\tau_{ij}$ ,  $S_{ij}$ ,  $C_s$ ,  $\Delta$  are the unresolved stress tensor, resolved strain tensor, Smagorinsky constant, and filter width respectively. Apparently, it is a second order model with  $\Delta^2$ . Other models are similar. If we use a sixth order compact scheme for LES without model (Implicit LES), we will get sixth order of accuracy. However, if we add the Smagorinsky subgrid model, our LES results will be degenerated to second order of accuracy, which is really bad. A carefully designed 6<sup>th</sup> order subgrid model may be needed for high order LES. Therefore, second order DNS, second order LES with second order subgrid models are not appropriate for DNS or LES.

Table 1 shows the orders obtained by different orders of schemes, which demonstrates the importance of high order numerical schemes for DNS/LES.

Table 1. Orders of DNS/LES approaches

Scheme	Truncation Errors	Comments
Second order DNS	$O(h^2)$	Bad
Second order LES +Second order subgrid model	$O(h^2)$ or up	Bad
Sixth order LES without subgrid model (ILES)	$O(h^6)$	Good
Sixth order LES with second order subgrid model	$O(h^2)$	Bad
Sixth order LES with sixth order subgrid model	$O(h^6)$ or up	Best

#### 1.4 Basic point of view on the scheme development

The 3-D time dependent Navier-Stokes equations in a general curvilinear coordinate can be written as

$$\frac{1}{J} \frac{\partial Q}{\partial t} + \frac{\partial(E - E_v)}{\partial \xi} + \frac{\partial(F - F_v)}{\partial \eta} + \frac{\partial(F - F_v)}{\partial \zeta} = 0\tag{1.4}$$

For 1-D conservation law, it will be:

$$\frac{\partial Q}{\partial t} + \frac{\partial E}{\partial \xi} = 0$$

(1.5)

The critical issue for high order CFD is to find an accurate approximation of derivatives for a given discrete data set. The computer does not know any physical process but accepts a discrete data set as input. The output is also a discrete data set. We measure the input data by slopes to determine it is smooth (slope is small), oscillatory (slope is large), and non-differentiable (or corner points which have slopes large on one side, but small on the other side), or, in other words, by a smoothness function, and then an appropriate numerical scheme is set up based on the feature of the discrete data set, but not the governing system. This is the basic view point for our new scheme development.

## 2. Technical Approach

### 2.1 ENO reconstruction function

For 1-D conservation laws:

$$u_t(x,t) + f_x(u(x,t)) = 0 \quad (2.1)$$

When a conservative approximation to the spatial derivative is applied, a semi-discrete conservative form of the equation (2.1) is described as follows:

$$\frac{du_j}{dt} = -\frac{1}{\Delta x}(\hat{f}_{j+(1/2)} - \hat{f}_{j-(1/2)}) \quad (2.2)$$

where  $f_j = \frac{1}{\Delta x} \int_{x_j-\Delta x/2}^{x_j+\Delta x/2} \hat{f}(\xi) d\xi$  and then  $(f_x)_j = -\frac{1}{\Delta x}(\hat{f}_{j+(1/2)} - \hat{f}_{j-(1/2)})$ . Note that  $f$  is the original function, but  $\hat{f}$  is the flux defined by the above integration which is an exact expression of the flux but is different from  $f$ .

Let  $H$  be the primitive function of  $\hat{f}$  defined below:

$$H(x_{j+(1/2)}) = \int_{-\infty}^{x_j+\Delta x/2} \hat{f}(\xi) d\xi = \sum_{i=-\infty}^{i=j} \int_{x_i-\Delta x/2}^{x_i+\Delta x/2} \hat{f}(\xi) d\xi = \Delta x \sum_{i=-\infty}^j f_i \quad (2.3)$$

$H$  is easy to be calculated, but is a discrete data set.

The numerical flux  $\hat{f}$  at the cell interfaces is the derivative of its primitive function  $H$ . i.e.:

$$\hat{f}_{j+(1/2)} = H'_{j+(1/2)} \quad (2.4)$$

All formulae given above are exact without approximations. However, the primitive function  $H$  is a discrete data set or discrete function and we have to use numerical method to get the derivatives, which will introduce numerical errors, or, in other words, order of accuracy.

This procedure,  $f \rightarrow H \rightarrow \hat{f} \rightarrow f'_x$ , is called reconstruction introduced by Shu & Osher (1988, 1989). There is one and only one problem left for numerical methods, which is how to solve (2.4) or how to get accurate derivatives for a data set.

### 2.2 Data normalization

In order to find universal formula, we need to normalize the data set,  $u(i)$ ,  $i=1, \dots, n$ :

$$u_{diff} = |u_{\max} - u_{\min}| \quad (2.5)$$

$$\bar{u} = (u - u_{\min}) / u_{diff} \quad (2.6)$$

Here,  $u_{\max}$  and  $u_{\min}$  are the maximum and minimum values of  $u$  respectively and  $\bar{u}$  is normalized. For simplicity, we throw out the hat of  $u$  and use  $u(i)$  as the normalized data set.

### 2.3 Weighted compact scheme

As we addressed that there is one and only one problem left for numerical methods, which is how to solve (2.4) or how to get accurate derivatives for a discrete data set. It is equivalent to finding an accurate flux in the interface. We turn our attention into finding a high order scheme which, however, must be able to pass the shock without non-physical wiggles.

#### 2.3.1 WENO Scheme (Jiang & Su, 1996)

Before discuss our new scheme, first let us see how to construct the WENO scheme.

##### 2.3.1.1 Conservation Form of Derivative

$$\frac{\partial U}{\partial t} + \frac{\partial F}{\partial x} = 0 \quad (2.7)$$

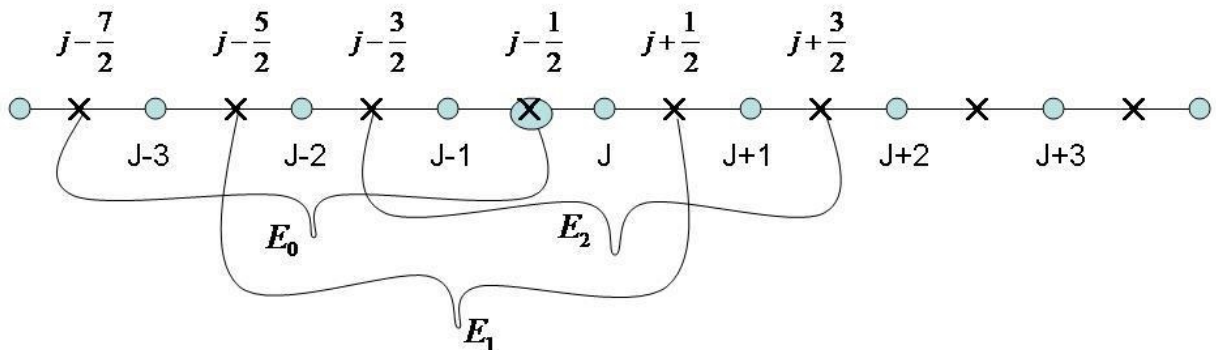
The ENO reconstruction can provide a semi-discretization for the derivative:  $\frac{\partial F}{\partial x} = \frac{\hat{F}_{i+\frac{1}{2}} - \hat{F}_{i-\frac{1}{2}}}{\Delta x}$ , where  $\hat{F}$  is the flux which must be accurately obtained.

##### 2.3.1.2 5<sup>th</sup> Order WENO (bias upwind)

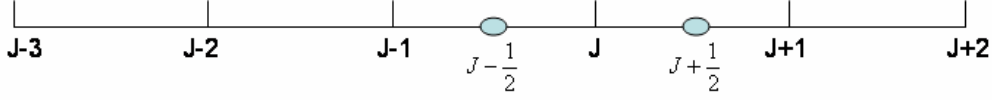
###### 1) Flux approximation

In order to get an high order approximation for  $\hat{F}_{j-\frac{1}{2}} = H'_{j-\frac{1}{2}}$ , we can use three different candidates (Figure 2.1) which are all third order polynomials:  $E_0 : H_{j-\frac{7}{2}}, H_{j-\frac{5}{2}}, H_{j-\frac{3}{2}}, H_{j-\frac{1}{2}}$ ;

$E_1 : H_{j-\frac{5}{2}}, H_{j-\frac{3}{2}}, H_{j-\frac{1}{2}}, H_{j+\frac{1}{2}}$ ;  $E_2 : H_{j-\frac{3}{2}}, H_{j-\frac{1}{2}}, H_{j+\frac{1}{2}}, H_{j+\frac{3}{2}}$ .



(a)



(b)

Figure 2.1 (a) WENO candidates (b) 5<sup>th</sup> order WENO SchemeLet us look at candidate  $E_0$  first. Assume  $H$  is a third order polynomial: $H = a_0 + a_1(x - x_{j-1/2}) + a_2(x - x_{j-1/2})^2 + a_3(x - x_{j-3/2})^3$ , we have

$$H_{j-1/2} = a_0$$

$$H_{j-3/2} = a_0 - a_1h + a_2h^2 - a_3h^3$$

$$H_{j-5/2} = a_0 - 2a_1h + 4a_2h^2 - 8a_3h^3$$

$$H_{j-7/2} = a_0 - 3a_1h + 9a_2h^2 - 27a_3h^3$$

(2.8)

Further by subtraction, we can get

$$H_{j-1/2} - H_{j-3/2} = hF_{j-1} = a_1h - a_2h^2 + a_3h^3$$

$$H_{j-1/2} - H_{j-5/2} = h(F_{j-1} + F_{j-2}) = 2a_1h - 4a_2h^2 + 8a_3h^3$$

(2.9)

$$H_{j-1/2} - H_{j-7/2} = h(F_{j-1} + F_{j-2} + F_{j-3}) = 3a_1h - 9a_2h^2 + 27a_3h^3$$

Deleting  $a_3$ , we can get

$$8F_{j-1} - (F_{j-1} + F_{j-2}) = 6a_1 - 4a_2h$$

$$27F_{j-1} - (F_{j-1} + F_{j-2} + F_{j-3}) = 24a_1 - 18a_2h$$

(2.10)

or

$$63F_{j-1} - 9F_{j-2} = 54a_1$$

$$52F_{j-1} - 2F_{j-2} - 2F_{j-3} = 48a_1$$

(2.11)

Then,

$$6a_1 = 2F_{j-3} - 7F_{j-2} + 11F_{j-1}$$

$$\text{Or } E_0 : \hat{F}_{j-1/2} = H_{j-1/2} = a_1 = \frac{1}{3}F_{j-3} - \frac{7}{6}F_{j-2} + \frac{11}{6}F_{j-1}$$

(2.12)

Finally, we have

$$E_0 : \hat{F}_{j-1/2} = \frac{1}{3}F_{j-3} - \frac{7}{6}F_{j-2} + \frac{11}{6}F_{j-1}$$

$$E_1 : \hat{F}_{j-1/2} = -\frac{1}{6}F_{j-2} + \frac{5}{6}F_{j-1} + \frac{1}{3}F_j$$

(2.13)

$$E_2 : \hat{F}_{j-1/2} = \frac{1}{3}F_{j-1} + \frac{5}{6}F_j - \frac{1}{6}F_{j+1}$$

## 2) Optimal weights for high order of accuracy

The final scheme should be a combination of three candidates:  $E = C_0 E_0 + C_1 E_1 + C_2 E_2$

If we set  $C_0 = \frac{1}{10}$ ,  $C_1 = \frac{6}{10}$ ,  $C_2 = \frac{3}{10}$ , we will have

$$\begin{aligned}\hat{F}_{j-\frac{1}{2}} &= \frac{1}{30} F_{j-3} - \frac{13}{60} F_{j-2} + \frac{47}{60} F_{j-1} + \frac{27}{60} F_j - \frac{1}{20} F_{j+1} \\ \hat{F}_{j+\frac{1}{2}} &= \frac{1}{30} F_{j-2} - \frac{13}{60} F_{j-1} + \frac{47}{60} F_j + \frac{27}{60} F_{j+1} - \frac{1}{20} F_{j+2}\end{aligned}\quad (2.14)$$

$$\frac{\partial F}{\partial x} = \frac{\hat{F}_{j+\frac{1}{2}} - \hat{F}_{j-\frac{1}{2}}}{\Delta x} = \left(-\frac{1}{30} F_{j-3} + \frac{1}{4} F_{j-2} - F_{j-1} + \frac{1}{3} F_j + \frac{1}{2} F_{j+1} - \frac{1}{20} F_{j+2}\right) / \Delta x + O(\Delta x^5)$$

Using Taylor expansion for  $F_{j-k}$ , we find

$$\frac{\partial F}{\partial x} = \frac{\hat{F}_{j+\frac{1}{2}} - \hat{F}_{j-\frac{1}{2}}}{\Delta x} = F'_j - \frac{1}{60} (\Delta x)^5 F_j^{(6)} + \frac{1}{140} (\Delta x)^6 F_j^{(7)} + \dots, \quad (2.15)$$

which shows the scheme with optimal weights and 6 grid points has a 5<sup>th</sup> order truncation error. Note that the scheme is a **STANDARD** 5<sup>th</sup> order bias upwind finite difference scheme.

### 3) Bias up-wind weights:

Let us define a bias weight for each candidate according to WENO:

$$\omega_k = \frac{\gamma_k}{\sum_{i=0}^2 \gamma_i}, \quad \gamma_k = \frac{C_k}{(\mathcal{E} + IS_k)^p} \quad (2.16)$$

where

$$\begin{aligned}IS_i &= \int_{x_{j-1/2}}^{x_{j+1/2}} \sum_{k=1}^{\infty} [p_2(x)^{(k)}]^2 h^{2k-1} dx \\ IS_0 &= \frac{13}{12} (F_{j-2} - 2F_{j-1} + F_j)^2 + \frac{1}{4} (F_{j-2} - 4F_{j-1} + 3F_j)^2 \\ IS_1 &= \frac{13}{12} (F_{j-1} - 2F_j + F_{j+1})^2 + \frac{1}{4} (F_{j-1} - F_{j+1})^2 \\ IS_2 &= \frac{13}{12} (F_j - 2F_{j+1} + F_{j+2})^2 + \frac{1}{4} (F_{j+2} - 4F_{j+1} + 3F_j)^2\end{aligned}$$

The 5<sup>th</sup> order WENO can be obtained

$$\hat{F}_{j-1/2} = \omega_0 E_0 + \omega_1 E_1 + \omega_2 E_2 \quad (2.17)$$

$$\begin{aligned}\hat{F}_{j-1/2} &= \omega_{0,j-1/2} \left(\frac{1}{3} F_{j-3} - \frac{7}{6} F_{j-2} + \frac{11}{6} F_{j-1}\right) + \omega_{1,j-1/2} \left(-\frac{1}{6} F_{j-2} + \frac{5}{6} F_{j-1} + \frac{1}{3} F_j\right) \\ &\quad + \omega_{2,j-1/2} \left(\frac{1}{3} F_{j-1} + \frac{5}{6} F_j - \frac{1}{6} F_{j+1}\right)\end{aligned}\quad (2.18)$$

WENO is a great scheme with great successes by many users. However, the scheme has 5<sup>th</sup> order dissipation everywhere and third order dissipation near the shock and people in DNS/LES

community complain it is too dissipative for transition and turbulence. Let us turn into central and compact schemes for assistance.

### 2.3.2 Weighted Compact Scheme (WCS, Jiang et al, 2001)

#### 1) High-order compact schemes

A Pade-type compact scheme could be constructed based on the Hermite interpolation where both function and derivatives at grid points are involved, e.g. a fourth order finite difference scheme can be constructed if both the function and first order derivative are used at three grid points. For a function  $f$  we may write a compact scheme by using five grid points (Lele, 1992):

$$\beta_- f'_{j-2} + \alpha_- f'_{j-1} + f'_j + \alpha_+ f'_{j+1} + \beta_+ f'_{j+2} = (b_- f_{j-2} + a_- f_{j-1} + c f_j + a_+ f_{j+1} + b_+ f_{j+2}) / \Delta \xi \quad (2.19)$$

We can get 8<sup>th</sup> order of accuracy by using the above formula based on Taylor series.

If we use a symmetric and tri-diagonal system, by setting  $\beta_- = \beta_+ = 0$ , we can get a one parameter family of compact scheme (Lele, 1992):

$$\alpha f'_{i-1} + f'_i + \alpha f'_{i+1} = \left[ -\frac{1}{12}(4\alpha - 1)f_{i-2} - \frac{1}{3}(\alpha + 2)f_{j-1} + \frac{1}{3}(\alpha + 2)f_{j+1} + \frac{1}{12}(4\alpha - 1)f_{i+2} \right] / h \quad (2.20)$$

If  $\alpha = \frac{1}{3}$ , we will get a standard sixth order compact scheme.

When a compact scheme is used to differentiate a discontinuous or shock function, the computed derivative has grid to grid oscillations. In our previous work (Jiang et al, 2001) we proposed a new class of finite difference scheme - weighted compact scheme (WCS).

#### 2) Basic formulations of weighted compact scheme

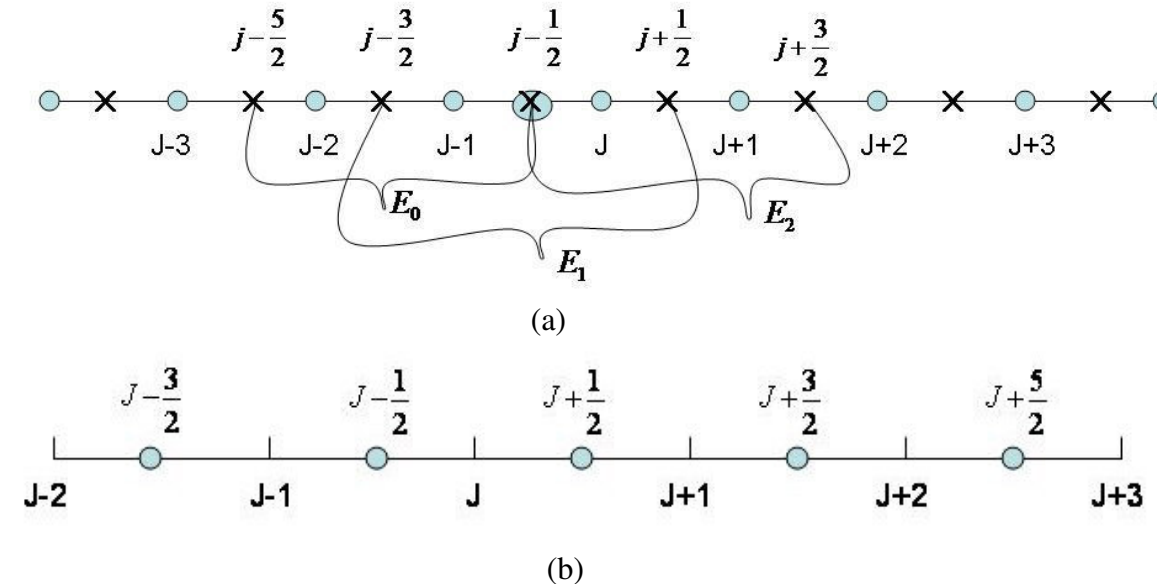


Figure 2.2 (a) WCS Stencil Candidates (b) Sixth Order Compact Scheme

In order to get an high order approximation for  $\hat{F}_{j-\frac{1}{2}} = H'_{j-\frac{1}{2}}$ , the six order weighted compact scheme uses three candidates for  $\hat{F}_{j-\frac{1}{2}}$  as shown in Figure 2.2 (a) which are all polynomials:

$$E_0 : H_{j-5/2}, H_{j-3/2}, H_{j-1/2}, E_1 : H_{j-3/2}, H_{j-1/2}, H_{j+1/2}, \text{ and } E_2 : H_{j-1/2}, H_{j+1/2}, F_{j+3/2} \quad (2.21)$$

Note that:

$$H_{j-1/2} = \sum_{i=0}^{j-1} F_i \Delta x \quad (2.22)$$

Compact schemes are used for these three candidates:

$$\begin{aligned} E_0 : \alpha_0 H'_{j-3/2} + H'_{j-1/2} &= (-b_0 H_{j-5/2} - a_0 H_{j-3/2} + c_0 H_{j-1/2}) / \Delta x \\ E_1 : \alpha_1 H'_{j-3/2} + H'_{j-1/2} + \alpha_1 H'_{j+1/2} &= a_1 (H_{j+1/2} - H_{j-3/2}) / \Delta x \\ E_2 : H'_{j-1/2} + \alpha_2 H'_{j+1/2} &= (b_2 H_{j+3/2} + a_2 H_{j+1/2} - c_2 H_{j-1/2}) / \Delta x \end{aligned} \quad (2.23)$$

For high order, we pick

$$\alpha_0 = 2, \alpha_1 = \frac{1}{4}, \alpha_2 = 2, a_0 = 2, a_1 = \frac{3}{4}, a_2 = 2, b_0 = \frac{1}{2}, b_2 = \frac{1}{2}, c_0 = \frac{5}{2}, c_2 = \frac{5}{2} \quad (2.24)$$

$E_0$  and  $E_2$  have third order, but  $E_1$  has fourth order of accuracy.

The compact scheme for each candidate is:

$$\begin{aligned} E_0 : 2H'_{j-3/2} + H'_{j-1/2} &= \left( -\frac{1}{2} H_{j-5/2} - 2H_{j-3/2} + \frac{5}{2} H_{j-1/2} \right) / h = \frac{5}{2} F_{j-1} + \frac{1}{2} F_{j-2} \\ E_1 : \frac{1}{4} H'_{j-3/2} + H'_{j-1/2} + \frac{1}{4} H'_{j+1/2} &= \frac{3(H_{j+1/2} - H_{j-3/2})}{4h} = \frac{3}{4} (F_j + F_{j-1}) \\ E_2 : H'_{j-1/2} + 2H'_{j+1/2} &= \left( \frac{1}{2} H_{j+3/2} + 2H_{j+1/2} - \frac{5}{2} H_{j-1/2} \right) / h = \frac{1}{2} F_{j+1} + \frac{5}{2} F_j \end{aligned} \quad (2.25)$$

3) Non-bias compact scheme

Let  $E = C_0 E_0 + C_1 E_1 + C_2 E_2$  and  $C_0 = \frac{1}{18}, C_1 = \frac{16}{18}, C_2 = \frac{1}{18}$

$$E : \frac{1}{3} H'_{j-3/2} + H'_{j-1/2} + \frac{1}{3} H'_{j+1/2} = \frac{1}{36} F_{j-2} + \frac{29}{36} F_{j-1} + \frac{29}{36} F_j + \frac{1}{36} F_{j+1} \quad (2.26)$$

Similarly, E at point  $j+1/2$  is

$$\frac{1}{3} H'_{j-1/2} + H'_{j+1/2} + \frac{1}{3} H'_{j+3/2} = \frac{1}{36} F_{j-1} + \frac{29}{36} F_j + \frac{29}{36} F_{j+1} + \frac{1}{36} F_{j+2} \quad (2.27)$$

Subtracting the previous equation at point  $j-1/2$ , we get

$$\frac{1}{3} F'_{j-1} + F'_j + \frac{1}{3} F'_{j+1} = \frac{1}{h} \left( -\frac{1}{36} F_{j-2} - \frac{7}{9} F_{j-1} + \frac{7}{9} F_{j+1} + \frac{1}{36} F_{j+2} \right) \quad (2.28)$$

This is a **standard** sixth order compact scheme. The stencil candidates are  $E_0 : F_{j-2}, F_{j-1}, E_1 : F_{j-1}, F_j$ , and  $E_2 : F_j, F_{j+1}$  for  $H'_{j-1/2} = \hat{F}_{j-1/2}$ . This also shows the WCS uses smaller candidate stencils but gets higher accuracy comparing with the 5<sup>th</sup> order WENO.

The procedure described above implies that a sixth order centered compact scheme can be constructed by a combination of three lower order schemes. In order to achieve the non-oscillatory property, the WENO weights (Jiang et al., 1996) are introduced to determine new weights for each stencil. The weights are determined according to the smoothness of the function on each stencil. Following the WENO method, the new weights are defined as

$$\omega_k = \frac{\gamma_k}{\sum_{i=0}^2 \gamma_i} \quad \gamma_k = \frac{C_k}{(\varepsilon + IS_k)^p} \quad (2.29)$$

where  $\varepsilon$  is a small positive number to prevent the denominator becoming zero and p is a parameter to control the weighting. Actually, p is very sensitive to affect the weights. We set p as a function of smoothness instead of constant. When p=0, the 6<sup>th</sup> order standard compact scheme is recovered.  $IS_k$  is a smoothness measurement which is defined in (2.16). Through the Taylor expansion, it can be easily proved that in smooth regions the new weights  $\omega_k$  satisfy:

$$\begin{aligned} \omega_k &= C_k + O(h^2) \text{ and} \\ \omega_2 - \omega_0 &= O(h^3) \end{aligned} \quad (2.30)$$

The new scheme is formed using these new weights:

$$E = \omega_0 E_0 + \omega_1 E_1 + \omega_2 E_2 \quad (2.31)$$

The leading error of E is a combination of the leading errors of the original schemes, which is:

$$\left(\frac{1}{12}\omega_0 - \frac{1}{12}\omega_2\right)f^{(4)}h^3 + \left(-\frac{1}{15}\omega_0 + \frac{1}{120}\omega_1 - \frac{1}{15}\omega_2\right)f^{(5)}h^4 \quad (2.32)$$

When equation (2.30) is satisfied, the leading error of the new scheme can be written as  $O(h^6)$  and the new scheme remains its 6<sup>th</sup> order of accuracy.

### 2.3.3 Modified Weighted Compact Scheme MWCS)

It seems like the WCS scheme is super over WENO especially for the shock-turbulence interaction, where both discontinuity and small length scales are important, when it uses Hermite polynomials as its building block. It is sixth order in the smooth area with weights of  $\frac{1}{18}, \frac{8}{9}, \frac{1}{18}$  and 4<sup>th</sup> order near the shock with weights of 1, 0, 0. The WCS really obtain pretty good results for wave equation and Burger equation. However, it is not so favorable for Euler equation. For 1-D shock tube case, it generates wiggles before and after the shock. For 2-D it meets more difficulties and blows up frequently. The reason is apparently that the WCS scheme does not have enough dissipation around the shock, which causes wiggles. Because the scheme is non-dissipative and central, the wiggles cannot be dissipated after they are generated. Then, a second order filter is required to remove these wiggles. However, the second order filter is case-related and has adjustable constants. There is always a risk to reduce the order of calculation by using second order filter. In this consideration, we tried to modify the flux given by (2.33):

$$F_{mwcs} = \alpha(x)F_{wcs} + (1 - \alpha(x))F_{bias} \quad (2.33)$$

The bias flux can be obtained by up-wind or bias up-wind schemes and only play roles near the shock (corner points). For the purpose to keep high order, we use the 5<sup>th</sup> order WENO in current work as a flux modification. The advantage is that WCS and WENO can share the smoothness measurement and WENO has 5<sup>th</sup> order accuracy. From computational practice, WENO looks too dissipative inside the boundary layers, but not strong enough to capture the shock without oscillation. We really need to find a better and optimized modification by choosing new  $\alpha(x)$  and  $F_{bias}$

## 2.3.4 Comparison of WENO and MWCS

### 2.3.4.1 Comparison in computation

1) Shock tube

Let first take a shock tube problem to see how the WENO works. The governing equations are 1D Euler equations:

$$\frac{\partial U}{\partial t} + \frac{\partial F}{\partial x} = 0 \quad (2.34)$$

$$U = (\rho, \rho u, E)^T; \quad F = (\rho u, \rho u u + p, u(E + p))^T$$

The initial conditions are given as follows:

$$(\rho, u, p) = \begin{cases} (1, 0, 1), & x < 0; \\ (0.125, 0, 0.1) & x \geq 0. \end{cases} \quad (2.35)$$

To solve the Euler equations, Three step TVD Runge-Kutta is used in time marching and Lax-Friedrich flux vector splitting is used and the derivatives of splitting flux  $F^+$ ,  $F^-$  are calculated using WENO. From Figure 2.3, the shock is smeared before and after shock and the expansion wave is smeared and deformed. This shows WENO has too much dissipation and mistreated the expansion wave. We then use modified WCS and compare with WENO in Figure 2.4. Apparently, shock is sharper and expansion wave deformation is removed.

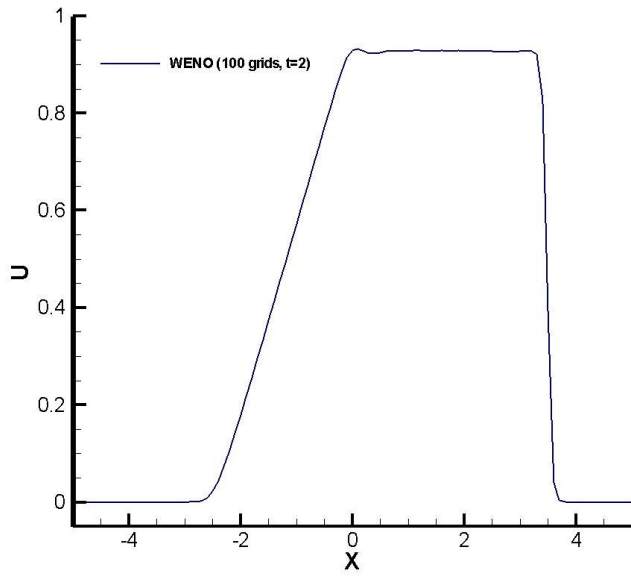


Figure 2.3 WENO for 1-D shock tube (T=2, grid=100)

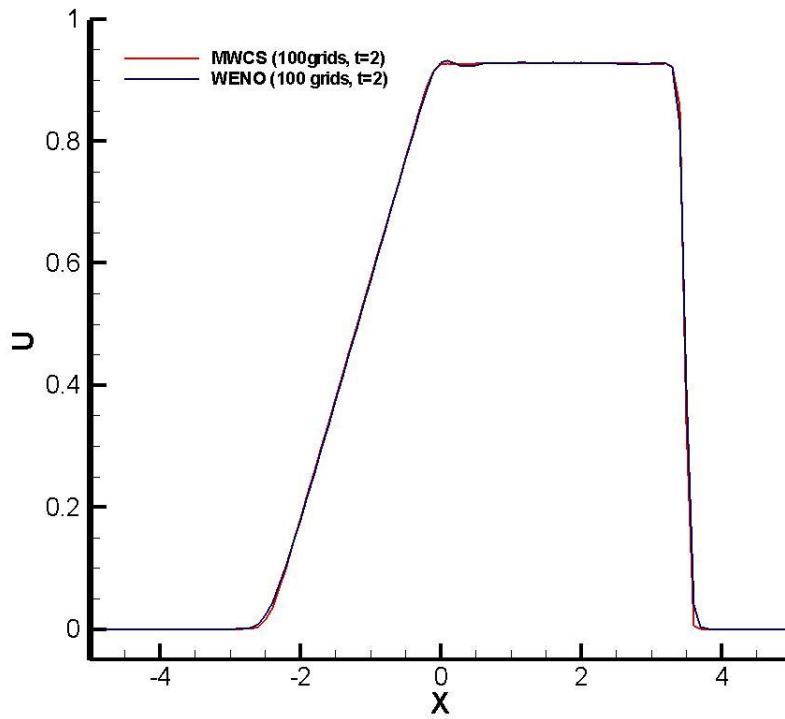


Figure 2.4 Modified WCS vs WENO for 1-D shock tube (T=2 and grids=100)

## 2) Shock-entropy interaction

To test the capability of the new scheme in both shock capturing and resolution, we applied it to the 1-D problem of shock/entropy wave interaction. In this case, Euler equations (2.25) are solved with the following initial conditions:

$$(\rho, u, p)_0 = \begin{cases} (3.857143, 2.629369, 10.33333), & x < -4; \\ (1 + 0.2 \sin(5x), 0, 1) & x \geq -4. \end{cases} \quad (2.36)$$

On a coarser grid with grid number of  $N=200$ , the MWCS (LJX) scheme shows much better resolution for small length scales than the 5<sup>th</sup> order WENO (Figure 2.5 (a), (b)). This is because MWCS uses central, non-dissipative, compact scheme with weights near the shock area and recovers high order compact right off the shock. The numerical results by our MWCS scheme with 200 grid points are even comparable with the 5<sup>th</sup> order WENO scheme with 1600 grid points (Figure 2.5 (b)).

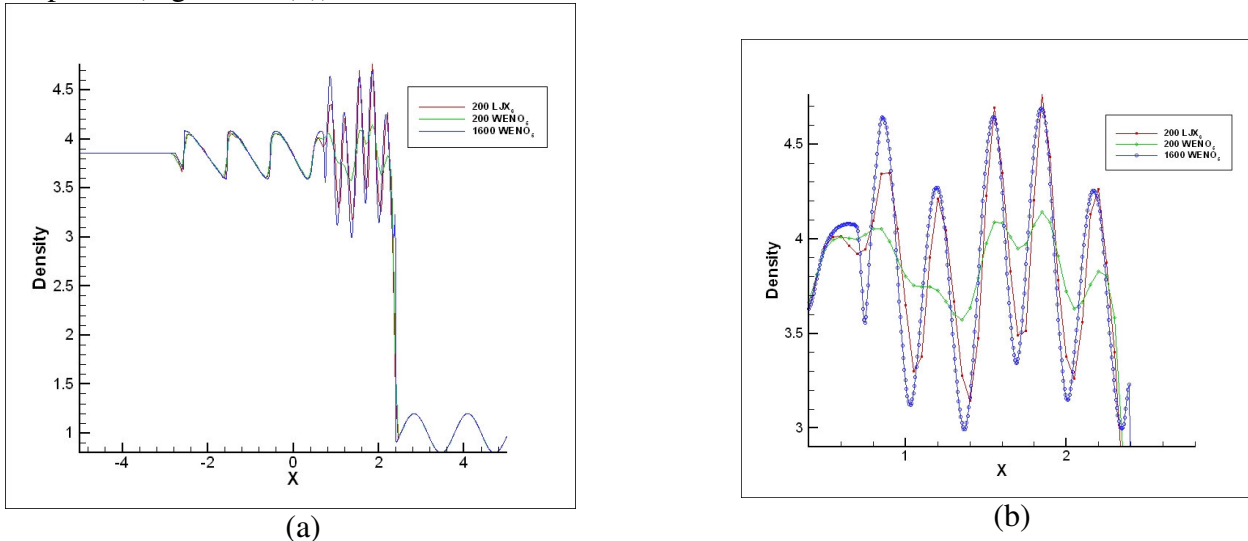


Figure 2.5 Numerical test for 1D shock-entropy wave interaction problem,  $t=1.8$ ,  $N=200$ . (b) is locally enlarged

### 2.3.4.2 Comparison in accuracy, dissipation, and dispersion

As shown in computation, the MWCS has much less dissipation than the 5<sup>th</sup> order WENO, we now provide some analytic analysis about the accuracy, dissipation and dispersion.

#### 1) Analysis of Local Truncation Error, Dissipation and Dispersion Terms:

##### a) 5<sup>th</sup> order WENO scheme:

The WENO scheme gives

$$\begin{aligned}
F'_j \approx \frac{\hat{F}_{j+\frac{1}{2}} - \hat{F}_{j-\frac{1}{2}}}{h} = & \left[ -\frac{1}{3}\omega_{0,j-1/2}F_{j-3} + \left( \frac{7}{6}\omega_{0,j-1/2} + \frac{1}{3}\omega_{0,j+1/2} + \frac{1}{6}\omega_{1,j-1/2} \right) F_{j-2} \right. \\
& + \left( -\frac{11}{6}\omega_{0,j-1/2} - \frac{7}{6}\omega_{0,j+1/2} - \frac{5}{6}\omega_{1,j-1/2} - \frac{1}{6}\omega_{1,j+1/2} - \frac{1}{3}\omega_{2,j-1/2} \right) F_{j-1} \\
& + \left( \frac{11}{6}\omega_{0,j+1/2} - \frac{1}{3}\omega_{1,j-1/2} + \frac{5}{6}\omega_{1,j+1/2} - \frac{5}{6}\omega_{2,j-1/2} + \frac{1}{3}\omega_{2,j+1/2} \right) F_j \\
& \left. + \left( \frac{1}{3}\omega_{1,j+1/2} + \frac{1}{6}\omega_{2,j-1/2} + \frac{5}{6}\omega_{2,j+1/2} \right) F_{j+1} - \frac{1}{6}\omega_{2,j+1/2}F_{j+2} \right] / h
\end{aligned} \tag{2.37}$$

By using the Taylor series expansion around  $j$ , the truncation error  $\tau_{WENO}$  of is

$$\begin{aligned}
\tau_{WENO} = & \left( \frac{(\omega_{0,j-1/2} - \omega_{0,j+1/2}) - (\omega_{1,j-1/2} - \omega_{1,j+1/2})}{6} \right) (h)^2 \frac{\partial^3 F_j}{\partial x^3} + \\
& + \left( \frac{(-61\omega_{0,j-1/2} + 25\omega_{0,j+1/2}) + (11\omega_{1,j-1/2} + \omega_{1,j+1/2}) - (\omega_{2,j-1/2} + 11\omega_{2,j+1/2})}{144} \right) (h)^3 \frac{\partial^4 F_j}{\partial x^4} + \\
& + \left( \frac{(91\omega_{0,j-1/2} - 19\omega_{0,j+1/2}) - (9\omega_{1,j-1/2} - \omega_{1,j+1/2}) + (\omega_{2,j-1/2} - 9\omega_{2,j+1/2})}{240} \right) (h)^4 \frac{\partial^5 F_j}{\partial x^5} + \\
& + \left( \frac{(-1021\omega_{0,j-1/2} + 121\omega_{0,j+1/2}) + (59\omega_{1,j-1/2} + \omega_{1,j+1/2}) - (\omega_{2,j-1/2} + 59\omega_{2,j+1/2})}{4320} \right) (h)^5 \frac{\partial^6 F_j}{\partial x^6} + \\
& + \left( \frac{(1163\omega_{0,j-1/2} - 83\omega_{0,j+1/2}) - (41\omega_{1,j-1/2} - \omega_{1,j+1/2}) + (\omega_{2,j-1/2} - 41\omega_{2,j+1/2})}{10080} \right) (h)^6 \frac{\partial^7 F_j}{\partial x^7} + \\
& + \left( \frac{(-11341\omega_{0,j-1/2} + 505\omega_{0,j+1/2}) + (251\omega_{1,j-1/2} + \omega_{1,j+1/2}) - (\omega_{2,j-1/2} + 251\omega_{2,j+1/2})}{241920} \right) (h)^7 \frac{\partial^8 F_j}{\partial x^8} + \\
& + \left( \frac{(11931\omega_{0,j-1/2} - 339\omega_{0,j+1/2}) - (169\omega_{1,j-1/2} - \omega_{1,j+1/2}) + (\omega_{2,j-1/2} - 169\omega_{2,j+1/2})}{725760} \right) (h)^8 \frac{\partial^9 F_j}{\partial x^9} + \\
& + \left( \frac{(-110941\omega_{0,j-1/2} + 2041\omega_{0,j+1/2}) + (1019\omega_{1,j-1/2} + \omega_{1,j+1/2}) - (\omega_{2,j-1/2} + 227\omega_{2,j+1/2})}{21772800} \right) (h)^9 \frac{\partial^{10} F_j}{\partial x^{10}} + \\
& + \dots
\end{aligned} \tag{2.38}$$

From (2.38), we can determine the dissipation error and the dispersion error, which are respectively the even derivative terms and the odd derivative terms of  $\tau_{WENO}$ :

Dissipation error:

$$\begin{aligned}
E_{WENO,dissip} = & \left( \frac{(-61\omega_{0,j-1/2} + 25\omega_{0,j+1/2}) + (11\omega_{1,j-1/2} + \omega_{1,j+1/2}) - (\omega_{2,j-1/2} + 11\omega_{2,j+1/2})}{144} \right) (h)^3 \frac{\partial^4 F_j}{\partial x^4} + \\
& + \left( \frac{(-1021\omega_{0,j-1/2} + 121\omega_{0,j+1/2}) + (59\omega_{1,j-1/2} + \omega_{1,j+1/2}) - (\omega_{2,j-1/2} + 59\omega_{2,j+1/2})}{4320} \right) (h)^5 \frac{\partial^6 F_j}{\partial x^6} + \\
& + \left( \frac{(-11341\omega_{0,j-1/2} + 505\omega_{0,j+1/2}) + (251\omega_{1,j-1/2} + \omega_{1,j+1/2}) - (\omega_{2,j-1/2} + 251\omega_{2,j+1/2})}{241920} \right) (h)^7 \frac{\partial^8 F_j}{\partial x^8} + \\
& + \left( \frac{(-110941\omega_{0,j-1/2} + 2041\omega_{0,j+1/2}) + (1019\omega_{1,j-1/2} + \omega_{1,j+1/2}) - (\omega_{2,j-1/2} + 227\omega_{2,j+1/2})}{21772800} \right) (h)^9 \frac{\partial^{10} F_j}{\partial x^{10}} + \\
& + \dots
\end{aligned} \tag{2.39}$$

Dispersion error:

$$\begin{aligned}
E_{WENO,disp} = & \left( \frac{(\omega_{0,j-1/2} - \omega_{0,j+1/2}) - (\omega_{1,j-1/2} - \omega_{1,j+1/2})}{6} \right) (h)^2 \frac{\partial^3 F_j}{\partial x^3} + \\
& + \left( \frac{(91\omega_{0,j-1/2} - 19\omega_{0,j+1/2}) - (9\omega_{1,j-1/2} - \omega_{1,j+1/2}) + (\omega_{2,j-1/2} - 9\omega_{2,j+1/2})}{240} \right) (h)^4 \frac{\partial^5 F_j}{\partial x^5} + \\
& + \left( \frac{(1163\omega_{0,j-1/2} - 83\omega_{0,j+1/2}) - (41\omega_{1,j-1/2} - \omega_{1,j+1/2}) + (\omega_{2,j-1/2} - 41\omega_{2,j+1/2})}{10080} \right) (h)^6 \frac{\partial^7 F_j}{\partial x^7} + \\
& + \left( \frac{(11931\omega_{0,j-1/2} - 339\omega_{0,j+1/2}) - (169\omega_{1,j-1/2} - \omega_{1,j+1/2}) + (\omega_{2,j-1/2} - 169\omega_{2,j+1/2})}{725760} \right) (h)^8 \frac{\partial^9 F_j}{\partial x^9} + \\
& + \dots
\end{aligned} \tag{2.40}$$

### b) Weighted Compact Scheme (WCS):

On a similar analysis for the WCS, we can get

$$\begin{aligned}
F'_j \approx & \frac{\hat{F}_{j+1/2} - \hat{F}_{j-1/2}}{h} = \\
& - \frac{\omega_{0,j-1/2}}{6h} F_{j-2} + \left( \frac{\omega_{0,j+1/2}}{6h} - \frac{5\omega_{0,j-1/2}}{6h} - \frac{\omega_{1,j-1/2}}{2h} \right) F_{j-1} + \\
& + \left( \frac{5\omega_{0,j+1/2}}{6h} + \frac{\omega_{1,j+1/2}}{2h} - \frac{\omega_{1,j-1/2}}{2h} - \frac{5\omega_{2,j-1/2}}{6h} \right) F_j + \\
& + \left( \frac{\omega_{1,j+1/2}}{2h} + \frac{5\omega_{2,j+1/2}}{6h} - \frac{\omega_{2,j-1/2}}{6h} \right) F_{j+1} + \frac{\omega_{2,j+1/2}}{6h} F_{j+2} - \left( \frac{2\omega_{0,j-1/2}}{3} + \frac{\omega_{1,j-1/2}}{6} \right) F'_{j-1} \\
& + \left( \frac{2\omega_{0,j+1/2}}{3} + \frac{\omega_{1,j+1/2}}{6} + \frac{\omega_{1,j-1/2}}{6} + \frac{2\omega_{2,j-1/2}}{3} \right) F'_j - \left( \frac{\omega_{1,j+1/2}}{6} + \frac{2\omega_{2,j+1/2}}{3} \right) F'_{j+1}
\end{aligned} \tag{2.41}$$

by using the Taylor series expansion around  $j$ , the truncation error  $\tau_{WCS}$  of is

$$\begin{aligned}
\tau_{WCS} = & \left( \frac{(\omega_{0,j-1/2} - \omega_{0,j+1/2}) - (\omega_{2,j-1/2} - \omega_{2,j+1/2})}{36} \right) (h)^2 \frac{\partial^3 F}{\partial x^3} + \\
& + \left( \frac{2(\omega_{0,j+1/2} - 3\omega_{0,j-1/2}) + 2(3\omega_{2,j+1/2} - \omega_{2,j-1/2})}{144} \right) (h)^3 \frac{\partial^4 F}{\partial x^4} + \\
& + \left( \frac{(17\omega_{0,j-1/2} - \omega_{0,j+1/2}) - 2(\omega_{1,j-1/2} + \omega_{1,j+1/2}) - (\omega_{2,j-1/2} - 17\omega_{2,j+1/2})}{720} \right) (h)^4 \frac{\partial^5 F}{\partial x^5} + \\
& + \left( \frac{4(\omega_{0,j+1/2} - 12\omega_{0,j-1/2}) + 4(12\omega_{2,j+1/2} - \omega_{2,j-1/2})}{4320} \right) (h)^5 \frac{\partial^6 F}{\partial x^6} + \\
& + \left( \frac{(105\omega_{0,j-1/2} - \omega_{0,j+1/2}) - 4(\omega_{1,j-1/2} + \omega_{1,j+1/2}) - (\omega_{2,j-1/2} - 105\omega_{2,j+1/2})}{30240} \right) (h)^6 \frac{\partial^7 F}{\partial x^7} + \\
& + \left( \frac{6(\omega_{0,j+1/2} - 39\omega_{0,j-1/2}) + 6(39\omega_{2,j+1/2} - \omega_{2,j-1/2})}{241920} \right) (h)^7 \frac{\partial^8 F}{\partial x^8} + \\
& + \left( \frac{(481\omega_{0,j-1/2} - \omega_{0,j+1/2}) - 6(\omega_{1,j-1/2} + \omega_{1,j+1/2}) - (\omega_{2,j-1/2} - 481\omega_{2,j+1/2})}{2177280} \right) (h)^8 \frac{\partial^9 F}{\partial x^9} + \\
& + \left( \frac{4(2\omega_{0,j+1/2} - 249\omega_{0,j-1/2}) + 4(249\omega_{2,j+1/2} - 2\omega_{2,j-1/2})}{21772800} \right) (h)^9 \frac{\partial^{10} F}{\partial x^{10}} + \\
& + \dots
\end{aligned} \tag{2.42}$$

From (2.42), we can determine the dissipation error and the dispersion error, which are respectively the even derivative terms and the odd derivative terms of  $\tau_{WCS}$ :

Dissipation error:

$$\begin{aligned}
E_{WCS,dissip} = & \left( \frac{2(\omega_{0,j+1/2} - 3\omega_{0,j-1/2}) + 2(3\omega_{2,j+1/2} - \omega_{2,j-1/2})}{144} \right) (h)^3 \frac{\partial^4 F}{\partial x^4} + \\
& + \left( \frac{4(\omega_{0,j+1/2} - 12\omega_{0,j-1/2}) + 4(12\omega_{2,j+1/2} - \omega_{2,j-1/2})}{4320} \right) (h)^5 \frac{\partial^6 F}{\partial x^6} + \\
& + \left( \frac{6(\omega_{0,j+1/2} - 39\omega_{0,j-1/2}) + 6(39\omega_{2,j+1/2} - \omega_{2,j-1/2})}{241920} \right) (h)^7 \frac{\partial^8 F}{\partial x^8} + \\
& + \left( \frac{4(2\omega_{0,j+1/2} - 249\omega_{0,j-1/2}) + 4(249\omega_{2,j+1/2} - 2\omega_{2,j-1/2})}{21772800} \right) (h)^9 \frac{\partial^{10} F}{\partial x^{10}} + \\
& + \dots
\end{aligned} \tag{2.43}$$

Dispersion error:

$$\begin{aligned}
E_{WCS,disp} = & \left( \frac{(\omega_{0,j-1/2} - \omega_{0,j+1/2}) - (\omega_{2,j-1/2} - \omega_{2,j+1/2})}{36} \right) (h)^2 \frac{\partial^3 F}{\partial x^3} + \\
& + \left( \frac{(17\omega_{0,j-1/2} - \omega_{0,j+1/2}) - 2(\omega_{1,j-1/2} + \omega_{1,j+1/2}) - (\omega_{2,j-1/2} - 17\omega_{2,j+1/2})}{720} \right) (h)^4 \frac{\partial^5 F}{\partial x^5} + \\
& + \left( \frac{(105\omega_{0,j-1/2} - \omega_{0,j+1/2}) - 4(\omega_{1,j-1/2} + \omega_{1,j+1/2}) - (\omega_{2,j-1/2} - 105\omega_{2,j+1/2})}{30240} \right) (h)^6 \frac{\partial^7 F}{\partial x^7} + \\
& + \left( \frac{(481\omega_{0,j-1/2} - \omega_{0,j+1/2}) - 6(\omega_{1,j-1/2} + \omega_{1,j+1/2}) - (\omega_{2,j-1/2} - 481\omega_{2,j+1/2})}{2177280} \right) (h)^8 \frac{\partial^9 F}{\partial x^9} + \\
& + \dots
\end{aligned} \tag{2.44}$$

## 2) Error Analysis

We now study the order of accuracy of WCS schemes. Apparently, the WENO will have 5<sup>th</sup> order accuracy and the WCS has 6<sup>th</sup> order in a smooth area. For the near shock area, the worst case is to have weights of 1,0,0. In such a circumstance, the WENO will be third order, but WCS is fourth since the left candidate is second order for WENO and third order for WCS.

**Theorem 1.** Assume eq. (2.1), a 1-D conservation law has a nonlinear function  $F$  that is differentiable up to 7<sup>th</sup> order and  $u(x,t)$  is a generalized solution of eq. (2.1). Then given any fixed bounded domain  $D \subset R^1$  and  $0 < t \leq T < \infty$  there exist  $h_0 = h_0(u) > 0$  such that for any mesh size  $\Delta x < h_0$ , WCS scheme in eq. (2.10) gives 6<sup>th</sup> order accuracy in smooth regions of  $u(x,t)$ , i.e.

$$F_x - (\hat{F}_{j+\frac{1}{2}} - \hat{F}_{j-\frac{1}{2}}) / \Delta x = O(\Delta x^6), \text{ and they achieve essentially non-oscillatory property.}$$

The proof is skipped here due to the limit in length

## 3) Fourier Analysis for WCS and WENO:

A Fourier analysis of the errors associated with the WCS and WENO was performed, by assuming that the spatial variable  $x$  is periodic over the domain  $[0, L]$ , and  $h = L / N$ . By decomposing the  $F$ 's into their Fourier coefficients (see Lele, 1992 for details), the dissipation and the dispersion errors can be analyzed through the plots of modified wavenumber versus wavenumber, as seen below (Figure 2.6). Note that the WCS is less dispersive than WENO, and has no dissipation (as a property of being a centered scheme).

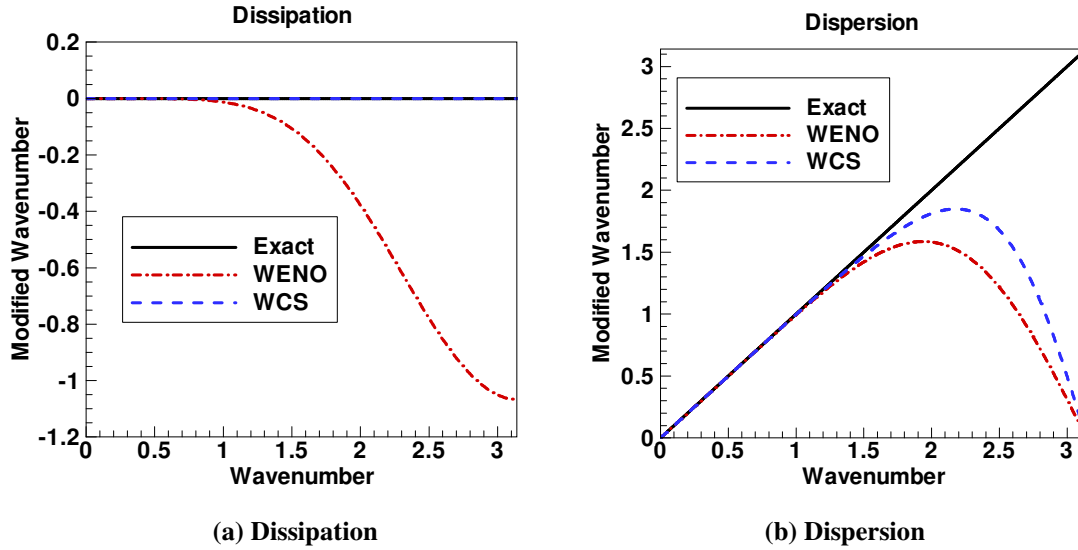


Figure 2.6 Dissipation and dispersion of WENO and WCS

#### 4) Analysis of weights:

We now proceed to analyze the weight functions for WCS.

**Proposition 2 .** Assume eq (2.1), a 1-D conservation law has a nonlinear function  $F$  that is differentiable up to 7<sup>th</sup> order and  $u(x,t)$  is a generalized solution of eq. (2.1). Then for any given fixed bounded domain  $D \subset \mathbb{R}^1$  and  $0 < t \leq T < \infty$  there exist  $h_0 = h_0(u) > 0$  such that for any mesh size  $\Delta x < h_0$ , WCS or WENO scheme gives a weight function  $\omega_i = c_i + O(\Delta x^4)$  for regions where  $u(x,t)$  and its derivatives (up to 4<sup>th</sup> order) are bounded. Otherwise,  $\omega_i = O(1)$ .

Again, the proof is skipped here due to the limit in length. All theoretical analyses and proofs have been documented in our recent three research papers which have been or will be submitted to scientific journal for review (Su et al, 2007).

##### a) Sinuous function

The results in the previous section are only applicable for continuous, smooth functions. Since the purpose of these numerical schemes is shock-capturing, then an analysis of the properties of the numerical schemes near a shock is necessary.

In a similar study as in section 2.3, the weights  $\omega_{0,j+1/2}$ ,  $\omega_{1,j+1/2}$ , and  $\omega_{2,j+1/2}$  of WENO and WCS are calculated for the function

$$f(x_j) = \begin{cases} \sin(2\pi x_j), & 0 \leq x_j \leq 0.5 \\ 1 - \sin(2\pi x_j), & 0.5 < x_j \leq 1 \end{cases} \quad (2.45)$$

plotted below, where  $x_j = j\Delta x$  and  $\Delta x = \frac{1}{40}$ .

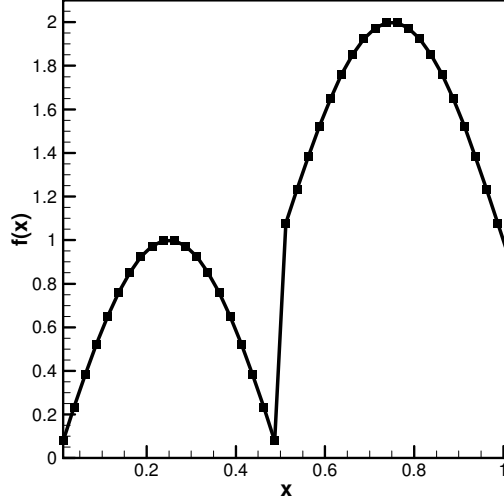


Figure 2.7 Sinuous function

The WENO and WCS weights ( $\omega_0$ ,  $\omega_1$ ,  $\omega_2$ ) were determined for the function graphed below, where  $x_j = j\Delta x$  and  $\Delta x = \frac{1}{40}$ . The weights were calculated at points  $x_{j+1/2}$ . the original WENO smoothness is applied:

$$IS_{0,j+1/2} = \frac{13}{12}(F_{j-2} - 2F_{j-1} + F_j)^2 + \frac{1}{4}(F_{j-2} - 4F_{j-1} + 3F_j)^2;$$

$$IS_{1,j+1/2} = \frac{13}{12}(F_{j-1} - 2F_j + F_{j+1})^2 + \frac{1}{4}(F_{j-1} - F_{j+1})^2;$$

$$IS_{2,j+1/2} = \frac{13}{12}(F_j - 2F_{j+1} + F_{j+2})^2 + \frac{1}{4}(F_{j+2} - 4F_{j+1} + 3F_j)^2,$$

In the plots below, only the weights  $\omega_{0,j+1/2}$ ,  $\omega_{1,j+1/2}$  and  $\omega_{2,j+1/2}$  are shown for WENO scheme and for the Weighted Compact Scheme (WCS). They both show similar behavior (due to using the same smoothness indicators). We observe that near critical points ( $x = 0.25$  and  $0.75$ ) the weights are not optimal (a small shift occurs), and so the numerical schemes do not achieve their maximum orders at those points especially for WENO. WCS shows some kind better. Also, near the discontinuity at  $x = 0.5$ , the weight  $\omega_{0,18+1/2}$  (left of the discontinuity) for the WCS is very close to the optimal value  $C_0$ , which is not observed for the WENO

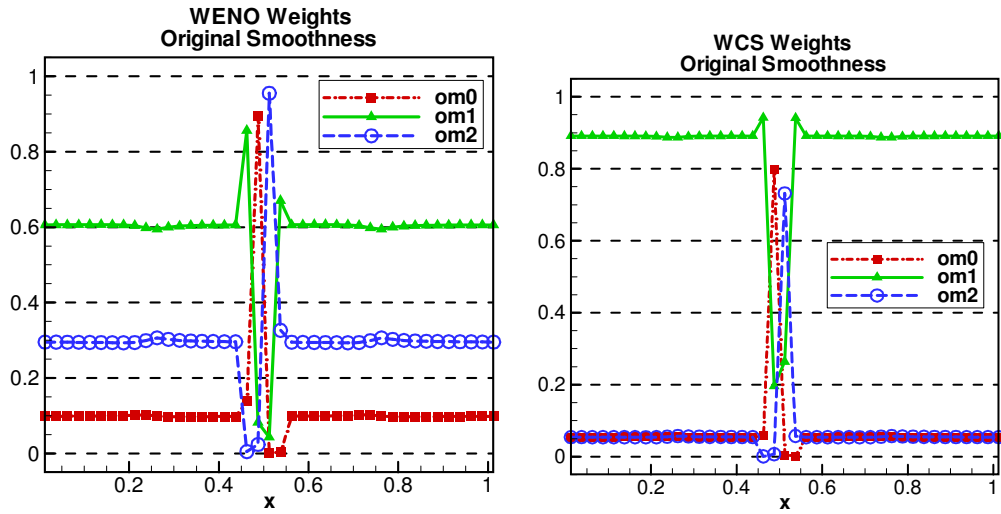


Figure 2.8 Weights of WENO and WCS for sinusoidal function

**b) Shock tube**

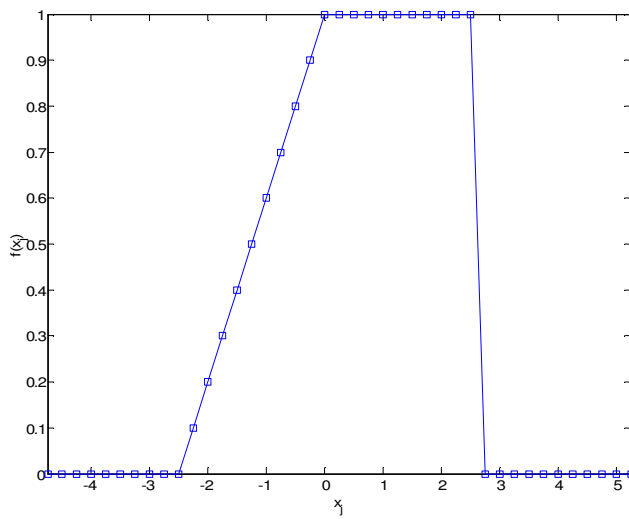


Figure 2.9 Shock tube function

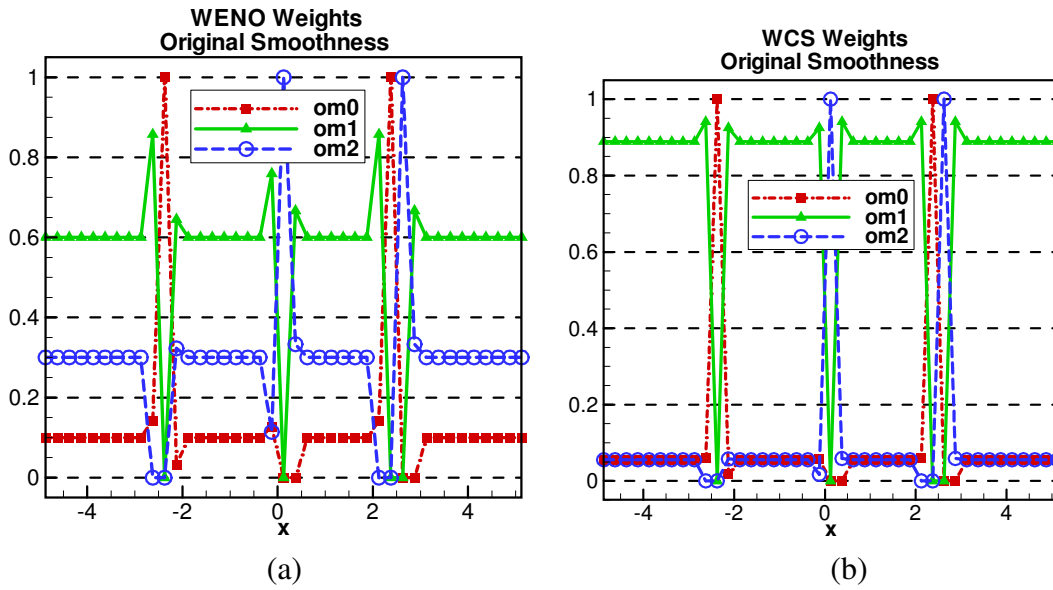


Figure 2.10 Weights of WENO and WCS for shock tube

Figure 2.9 and 2.10 show the weights for a shock tube. The weights keep optimal for high order accuracy, but jump near the shock and expansion wave. We note that the results at the expansion wave (between -2.5 and 0) are not considered smooth, and the weights are not the optimal weights. A similar result shows for WCS.

**c) Step function**

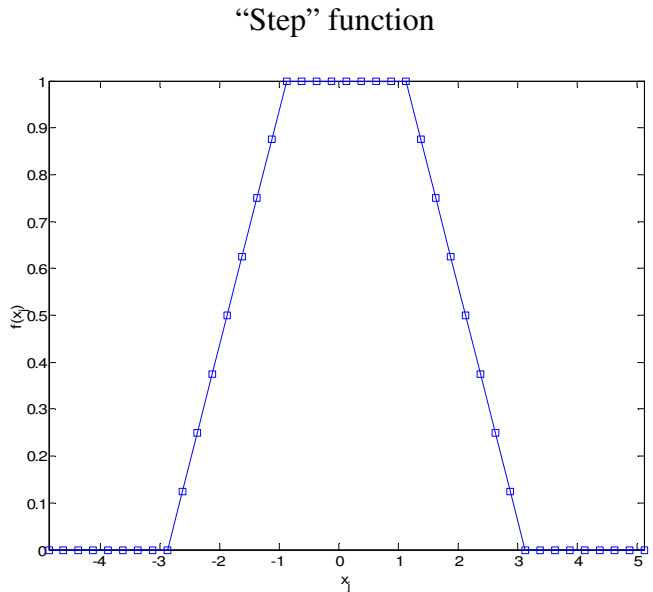
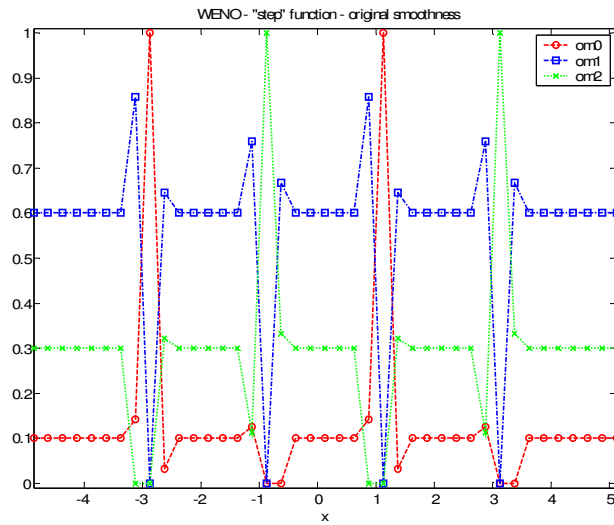
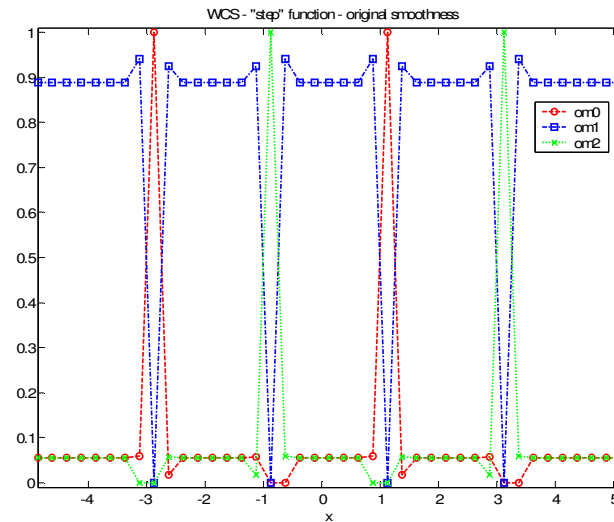


Figure 2.11 Step function



(a)



(b)

Figure 2.12 Weights of WENO (a) and WCS (b) for step function

Figure 2.11 and 2.12 show the weights for a step function. In all examples addressed above, the weights keep optimal for high order accuracy, but jump at four corner points (non-differentiable). This indicates that we only need to use bias weights at corner points. This analysis provides a hint that we may waste 95% of computation time. For example, when we use a thousand grid points but only have 4 corner points, why should we calculate smoothness and weights for a thousand grid points and solve the tri-diagonal system with variable coefficients at every time step? This will lead us to develop the version 3 of our black box subroutine with much high computation efficiency.

### 2.3.5 Black box subroutine

As addressed in previous sections, after ENO reconstruction, the remained problem is to find a more accurate derivative for a discrete data set. Based on this understanding, we developed a black box type subroutine which requires giving an input data set, the data dimension, and finite

difference direction. The subroutine will give back a discrete data as an output derivative. The idea is that this subroutine can work for any input data no matter it is smooth, oscillatory, or containing non-differentiable points. Of course, the subroutine should provide high order accuracy when the data is smooth. A black box type subroutine has been developed, applied in our own code, and delivered to Air Force Research Lab. This black box can be used anywhere or any finite difference CFD code. Of course, this is the first version and need to be improved.

### 2.3.6 Improvement of the algorithm and black box subroutine

We can make improvement to the black box type subroutine at least in several aspects:

#### 1) General Boundary conditions

The current one requires explicit boundary value at each time step which should be given by the finite difference CFD code. However, we can directly put the boundary conditions to this black box subroutine by defining:

$$af(x_b) + bf'(x_b) = c$$

The finite difference scheme will setup high order scheme for this point and the main program should provide value of a, b, and c. In real world, for a supersonic flow, we have inflow (Dirichlet, b=0), outflow (Neumann, a=0), far field and solid surface which could be Dirichlet, Neumann, or mixed depending on the sign of eigenvalue and heat transfer condition. The velocity on the wall is always zero and the boundary condition is Dirichlet. Therefore, the subroutine can self defined with high order for boundary points if the main program provide the parameters a, b and c for boundary conditions.

#### 2) Optimization of $F_{bias}$ and $\alpha$

As we apply modification to the flux obtained by WCS, we should optimize the  $F_{bias}$  and  $\alpha$

$$F_{mwcs} = \alpha(x)F_{wcs} + (1 - \alpha(x))F_{bias}$$

The desired  $F_{bias}$  should be able to capture strong shock (rapid change in slope) and the  $\alpha$  should control the introduction of  $F_{bias}$  and make sure no  $F_{bias}$  is introduced off shock and inside the boundary layer except for necessary high order dissipation. For a discrete data set, the strong shock will be considered as rapid change corner points and off shock boundary layer will be thought as smooth data set.

#### 3) Optimization of weights

The WCS is relied on weights to capture the shock and provide necessary dissipation for damping numerical wiggles. However, the current weights used by our scheme are WENO weights which shows strong up-winding at corner points and recover to non-bias weights off the shock quickly. Of course they are good weights, but not the best one. First, the computation shows the weights did not provide enough dissipation to capture the shock without wiggles that is why we still need  $F_{bias}$ . Second, the weights should provide necessary high order dissipation even in the smooth area since the WCS is non-dissipative scheme and cannot damp and existing numerical oscillations. Apparently, we need more work on the optimization of WCS weights

#### 4) Computation cost reduction

There are concerns which are naturally raised about the computation cost when so many technologies are used to construct the black box subroutine. However, a large part of cost will be dramatically reduced when we define a “corner point finder”. The solution is quite clear. Let us first look for two questions and answers. First one, why do we say WENO weights are good? The answer is because WENO weights become non-bias and standard weights to achieve high order. The second question is where the weights changed? The answer is the weight changes only near the corner points. Therefore, the answer is on our hand. It does not make much sense that we calculate the smoothness, find the weights, reconstruct our matrix, and then we did not change anything for most areas except a few corner points. It turns out we should develop some ways to isolate a few corner points (non-differentiable) and then modified our coefficients at these points. These will allow us to dramatically reduce the cost of WCS. In addition, if  $F_{bias}$  can be removed, even flux splitting is not necessary since WCS is central and does not require flux splitting. Really, we spend a lot of time and computation to calculate smoothness and find WENO weights, but finally we claim our scheme is very good because our weights are same as standard high order weights at most points except a few corner points (see above figures). It should be equivalent to make an adjustment at a few corner points and do nothing for all other points which will be much cheaper.

#### 5) Self flux splitting

At current time, we still need flux splitting since we use  $F_{bias}$ . In future, we plan to develop a Lax- Friedrich type flux splitting by the black box subroutine itself which will make the subroutine can treat any data sets no matter what kind governing system is involved.

### 3. Preliminary Results of the New Schemes

The 3-step, 3<sup>rd</sup> order TVD Runge-Kutta method is applied for time discretization.

#### 3.1 Order of Accuracy

The scheme is tested by solving a linear wave equation with a smooth initial function:

$$u_t + u_x = 0, \quad u(x,0) = \sin(2\pi x) \quad \text{where } 0 \leq x \leq 1. \quad (3.1)$$

The calculation stops at  $t = 0.3$  and the errors are listed in table 2. The computation shows the 6th order accuracy is achieved.

Table 2. Errors and Order of Accuracy

N	$L_1$ Error	$L_1$ Order	$L_2$ Error	$L_2$ Order	$L_\infty$ Error	$L_\infty$ Order
8	1.06E02	-	3.67E03	-	2.05E02	-
16	8.66E05	6.93	2.46E05	7.22	2.00E04	6.68
32	1.37E06	5.98	2.94E07	6.39	4.37E06	5.51
64	2.23E08	5.93	3.74E09	6.30	1.11E07	5.30
128	3.45E10	6.01	4.95E11	6.24	2.86E09	5.27
256	4.49E12	6.26	5.73E13	6.43	5.98E11	5.58

### 3.2. 1-D linear wave equation with jump initial function

The same governing equation is used but the initial condition is discontinuous:

$$u_t + u_x = 0, u(x,0) = \begin{cases} 1.0 & \text{if } 0.1 \leq x \leq 0.4 \\ 0.5 & \text{otherwise} \end{cases} \quad (3.2)$$

The calculation stops at  $t = 0.3$  and the solutions are illustrated in figure 3.1. The results indicate that standard compact scheme doesn't work for shocks while both MWCS (UWCNC) presented in this report and WENO scheme work. Furthermore, MWCS has less dissipation than WENO-5 near shocks which means a sharper transition is obtained.

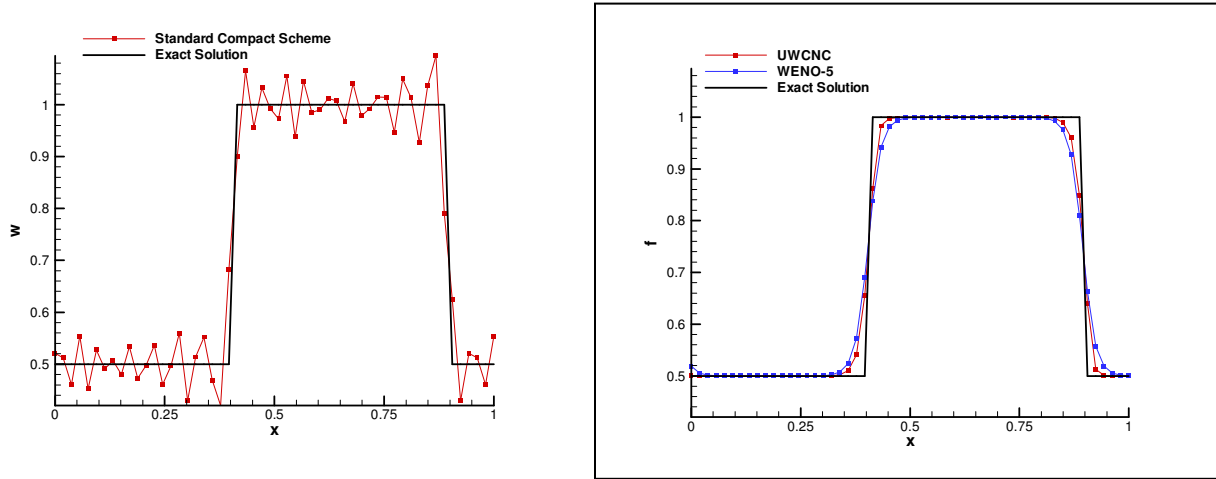


**Figure 3.1 Numerical test over linear wave equation.**

### 3.2 1-D shock tube and shock-entropy interaction

These results have been described in Chapter 2.

### 3.3 Preliminary results for 2-D shock-boundary layer interaction

In order to test if current MWCS scheme can work for 2-d and 3-D shock – boundary layer interaction. Three numerical tests are conducted: 1) incident shock; 2) double angles; 3) double cones. The case with double angles and double cone are still under numerical simulation and only the case with incident shock is reported here.

A 2-D incident shock-boundary layer interaction (Figure 3.2) was studied by the MWCS. The Reynolds number is  $10^5$  and the Mach number was set to 2.15. The overall pressure ratio is 1.55. For comparison, the inflow condition was set as same investigated by Degrez et al (1987). Their experimental work has shown the shock-boundary layer interaction is laminar and two-dimensional. Therefore, we can do a 2-D numerical simulation and compare with their computational and experimental results. The computational grids is  $257 \times 257$  (Figure 3.3). The grid stretching in streamwise direction is 1.01. The stretching in normal direction is 1.015. A 2-D Navier-Stokes equation is solved as the governing equation.

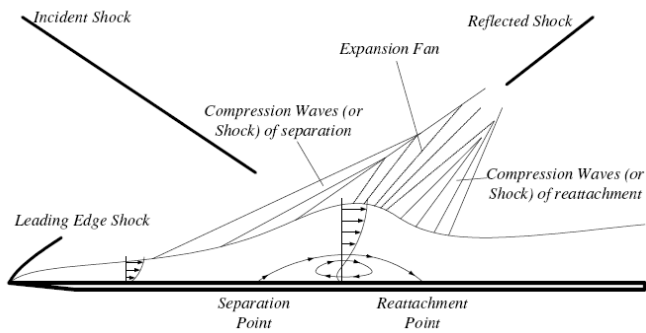


Figure 3.2 Sketch of incident shock-boundary layer interaction

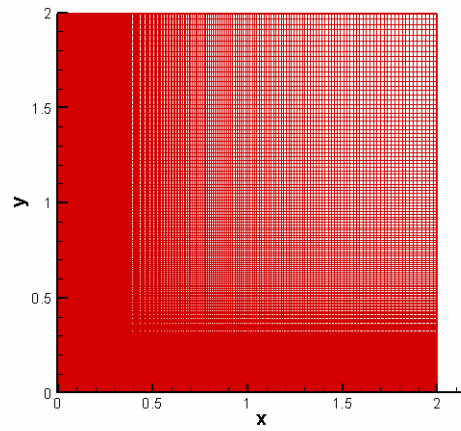


Figure 3.3 Computation Grids (257x257)

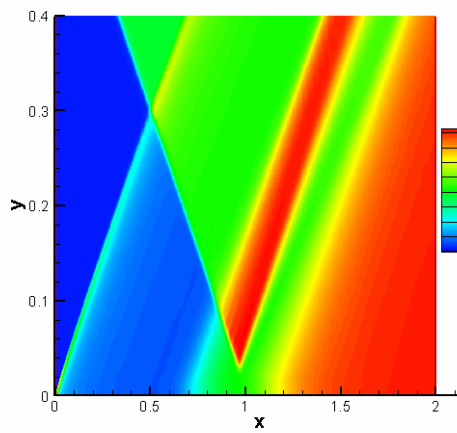
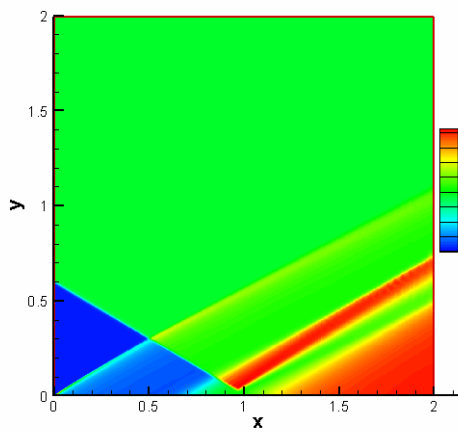


Figure 3.4 Pressure distribution: left is a normal view and right is stretched in the normal direction by a factor of 5

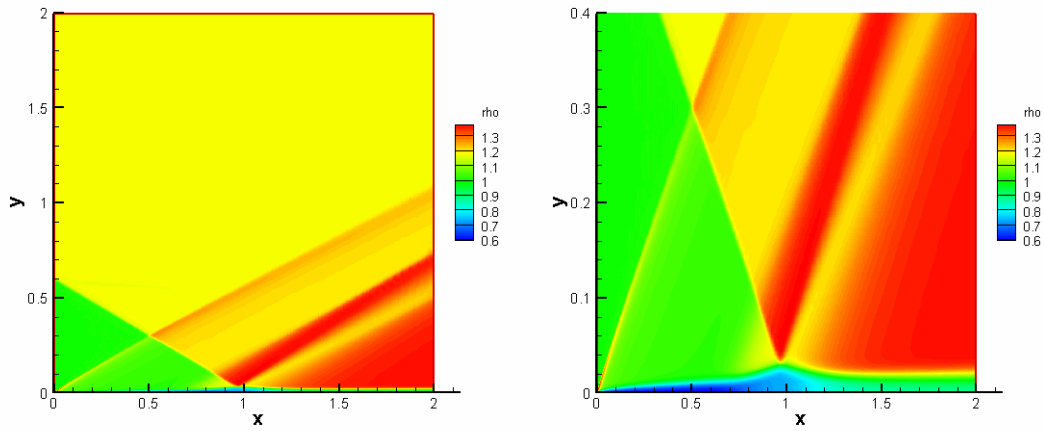


Figure 3.5 Density distribution: left is a normal view and right is stretched in the normal direction by a factor of 5

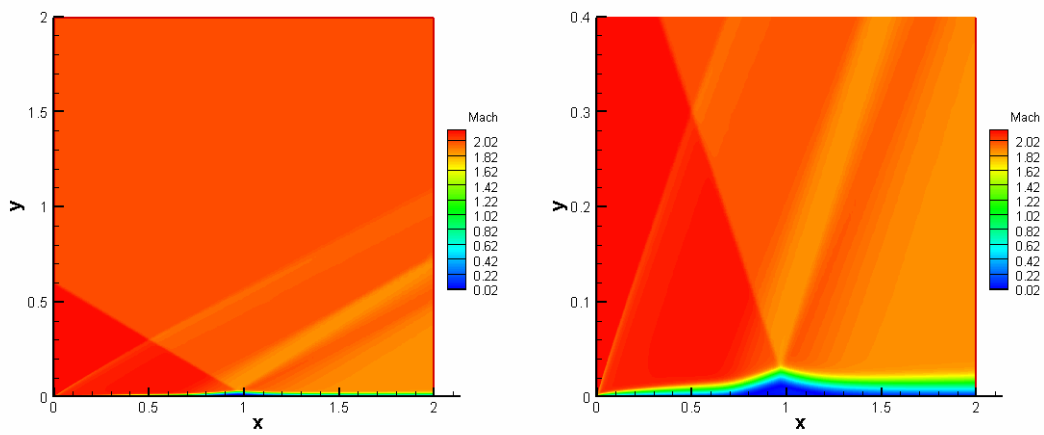


Figure 3.6 Mach number distribution: left is a normal view and right is stretched in the normal direction by a factor of 5

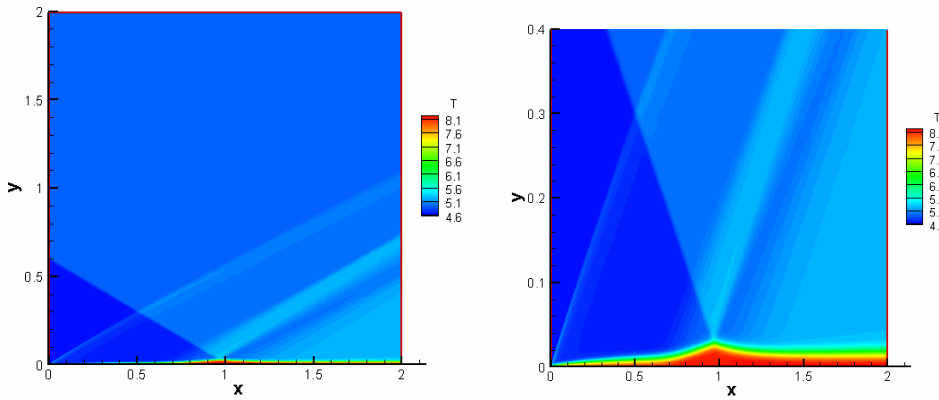


Figure 3.7 Temperature distribution: left is a normal view and right is stretched in the normal direction by a factor of 5

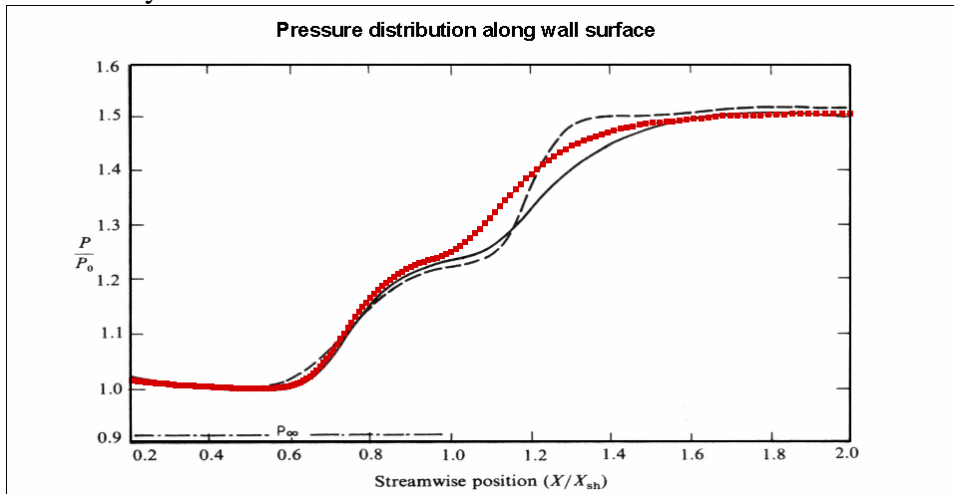


Figure 3.8 Comparison of pressure distribution on the wall surface. (The red one is our computation, the black dash one and solid one are Degrez's computation and experiment respectively)

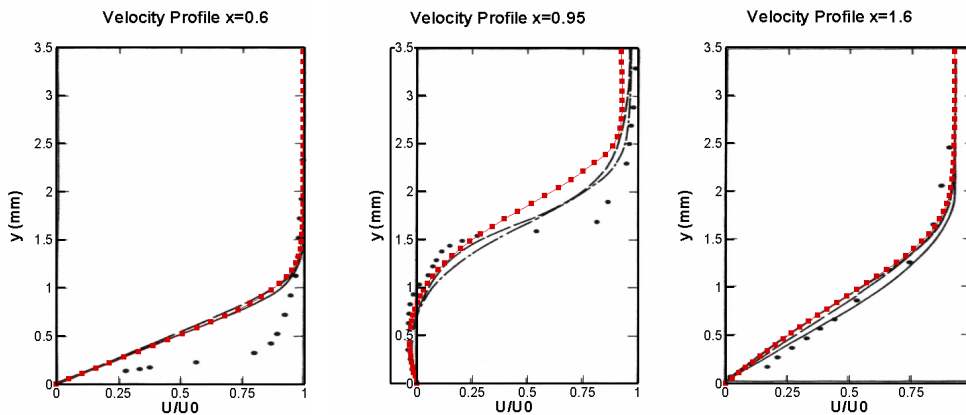


Figure 3.9 Comparison of velocity profiles at different locations (The red one is our computation, the black solid line and black square are Degrez's computation and experiment respectively)

Figures 3.4-3.7 show the distribution of pressure, density, Mach number and temperature obtained by our computation. Figure 3.8 and 3.9 show our numerical results agree well with the numerical results and are close to the experimental results given by Degrez et al (1987). Degrez et al favor their computational results addressed in their JFM paper. Figure 3.10 shows MWCS scheme has higher resolution for 2-D incident shock-boundary layer interaction. These results show our scheme can be extended to 2-D and 3-D problems.

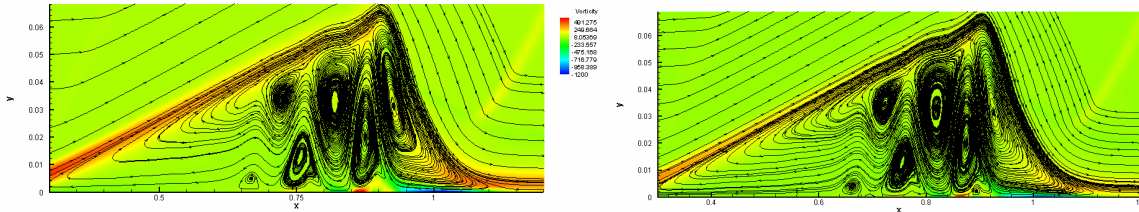
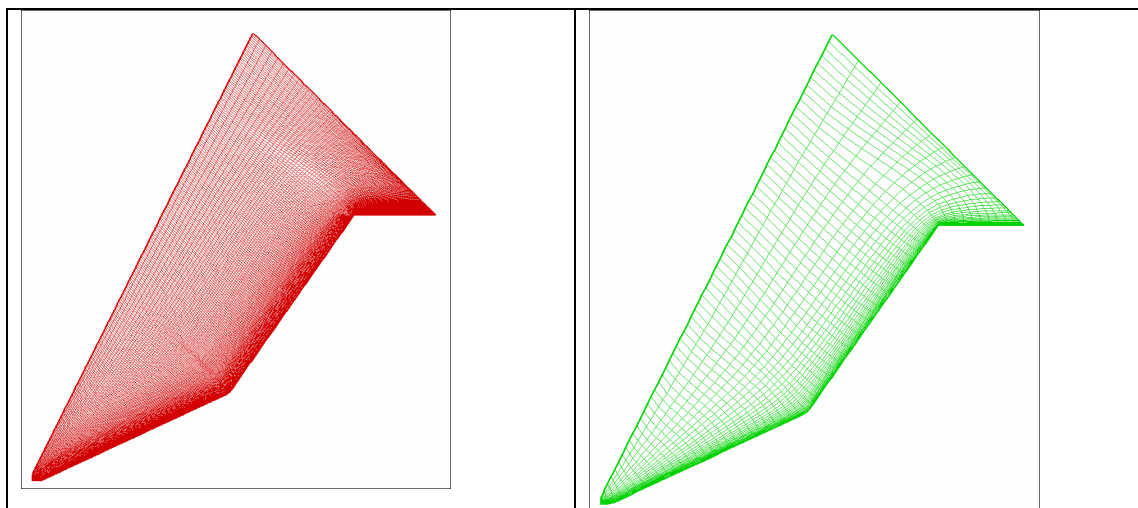


Figure 3.10 Vorticity of 2-D incident shock-boundary layer interaction: (a) WENO (b) MWCS

### 3.4 Preliminary results for 2-D double angle shock-boundary layer interaction at M=9.59

In order to validate our scheme and code, we should compare our results with well documented experimental and computational data. The case including the geometry and inflow condition was set same as the experiment conducted by Wadhams et al (2004) and the computation by Gaitonde et al (2002). The inflow Mach number is set to  $M=9.58$ , the Reynolds number  $Re=278870$ , the inflow temperature  $T_{in}=185.6$ , and the wall temperature  $T_w=293.3$ .

Before we work on a double cone, we solve a supersonic flow passing a double angle first. The overall Grid is  $257 \times 129$  obtained by elliptic grid generation and the grids are uniform in stream-wise direction, but stretched in wall normal direction with a factor of 1.037. The grids, contour of flow field and distribution of physical quantities along the wall boundary are shown in Figure 3.11-3.13. Since the case we calculated is for a double angle not a double cone, we cannot compare with the above experiment and computation directly for now. However, the distribution of mach number, pressure, density, and temperature are very similar. Further development will be set for double cones at  $M=9.59$  which will allow us to compare our computational results with the above experiment and computation.



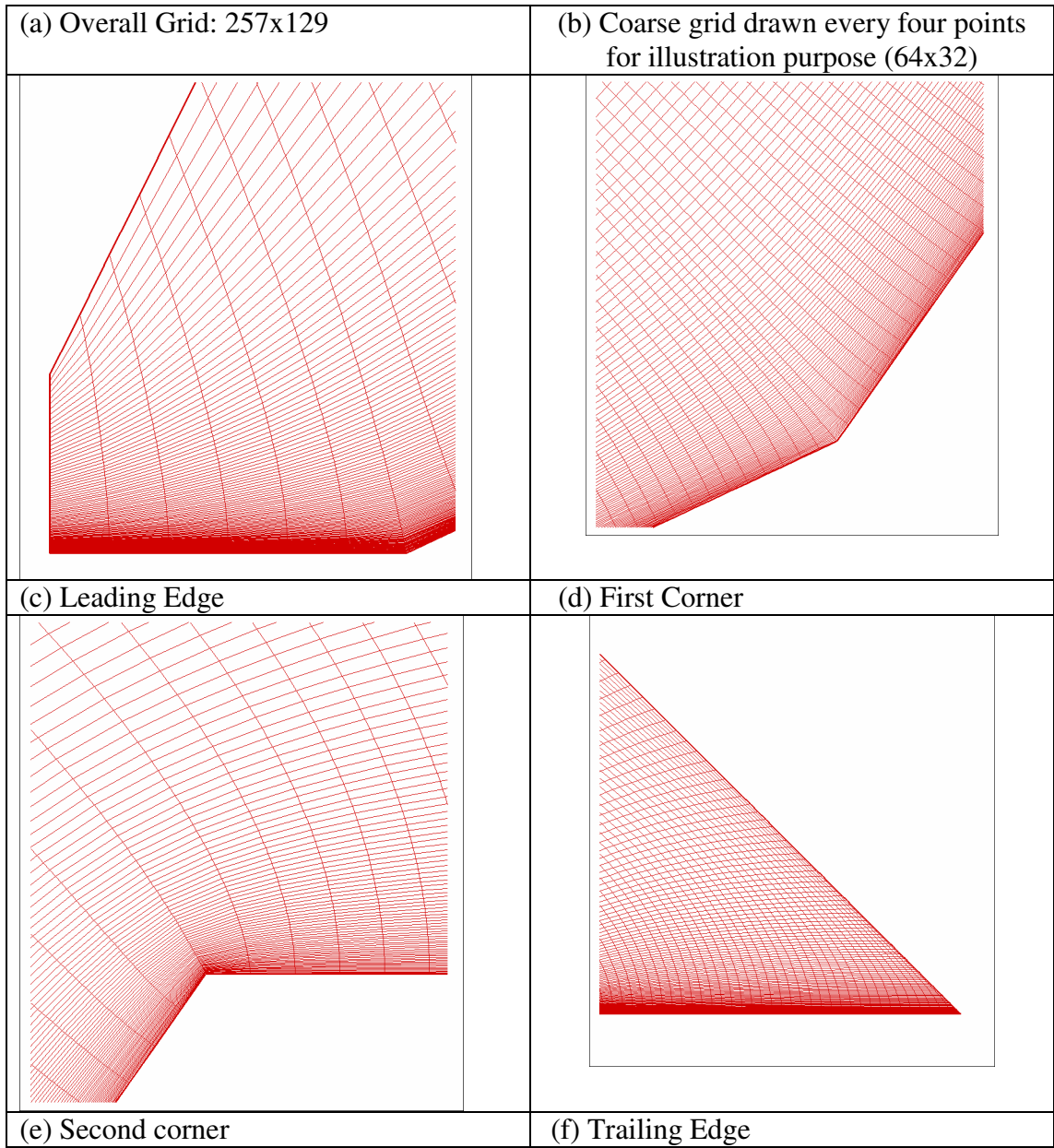


Figure 3.11. Elliptic Grid Generation

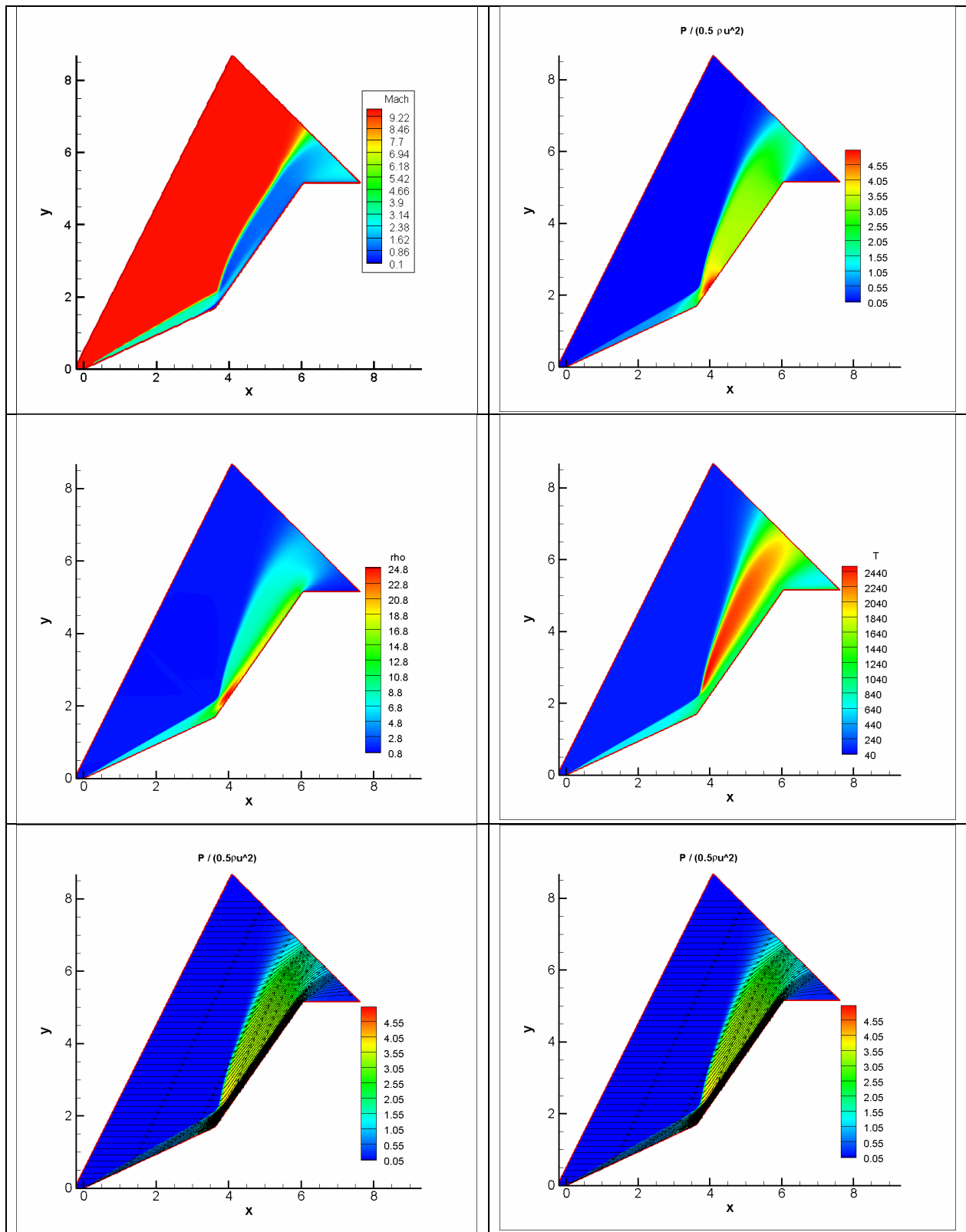


Figure 3.12. Contours of flow field (Mach number, pressure, density, temperature, stream line, and separation bubble)

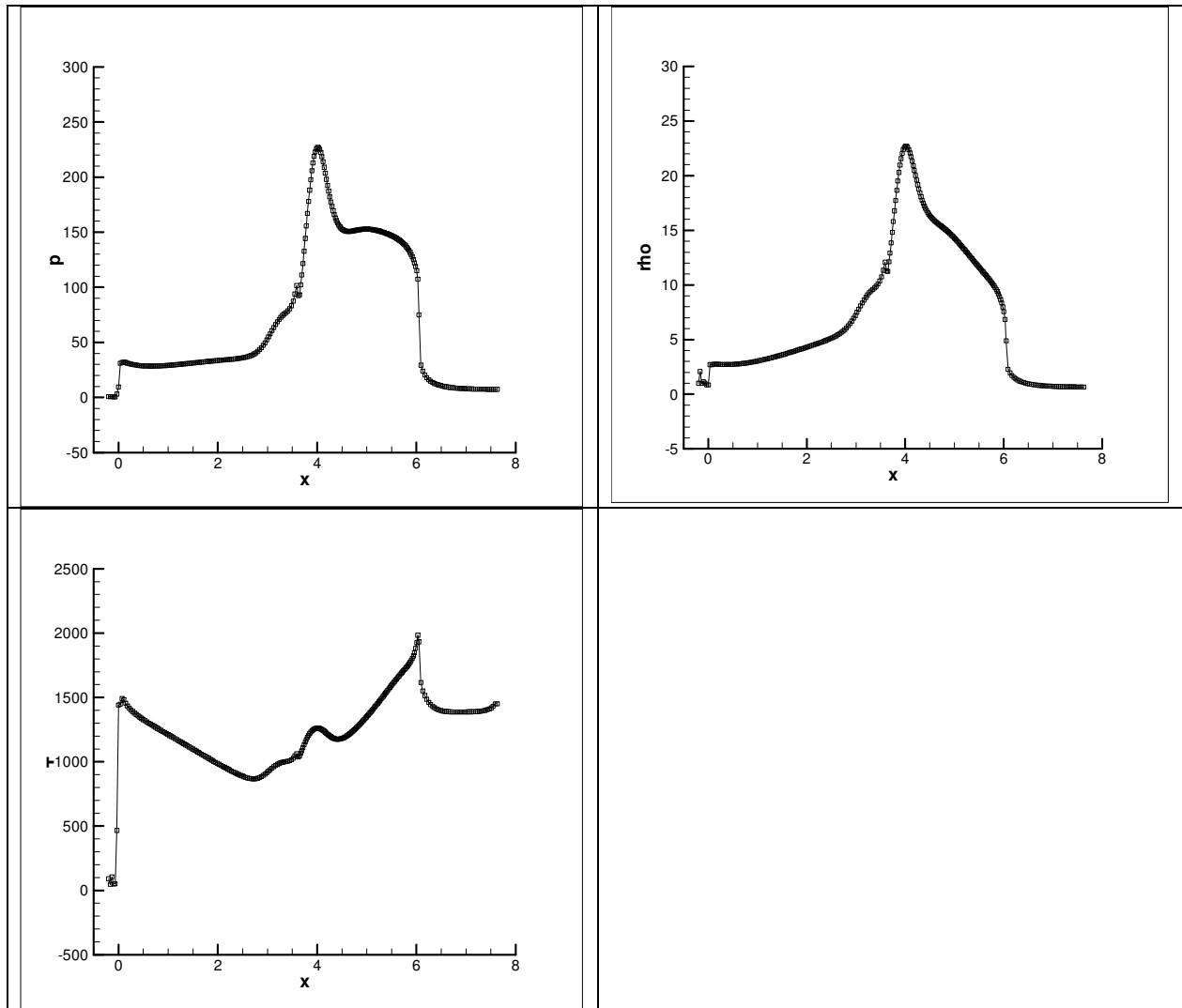


Figure 3.13 Distribution of physical quantities (pressure, density, and temperature) along the wall boundary:

Although we used same geometry and inflow conditions as the experiment (Wadhams et al, 2004) and the computation used, we cannot directly compare our results with theirs since their results are for double cones and ours for double angles. However, we can make qualitatively comparison and find the flow structure is very similar. Figure 3.14-3.17 show such a comparison.

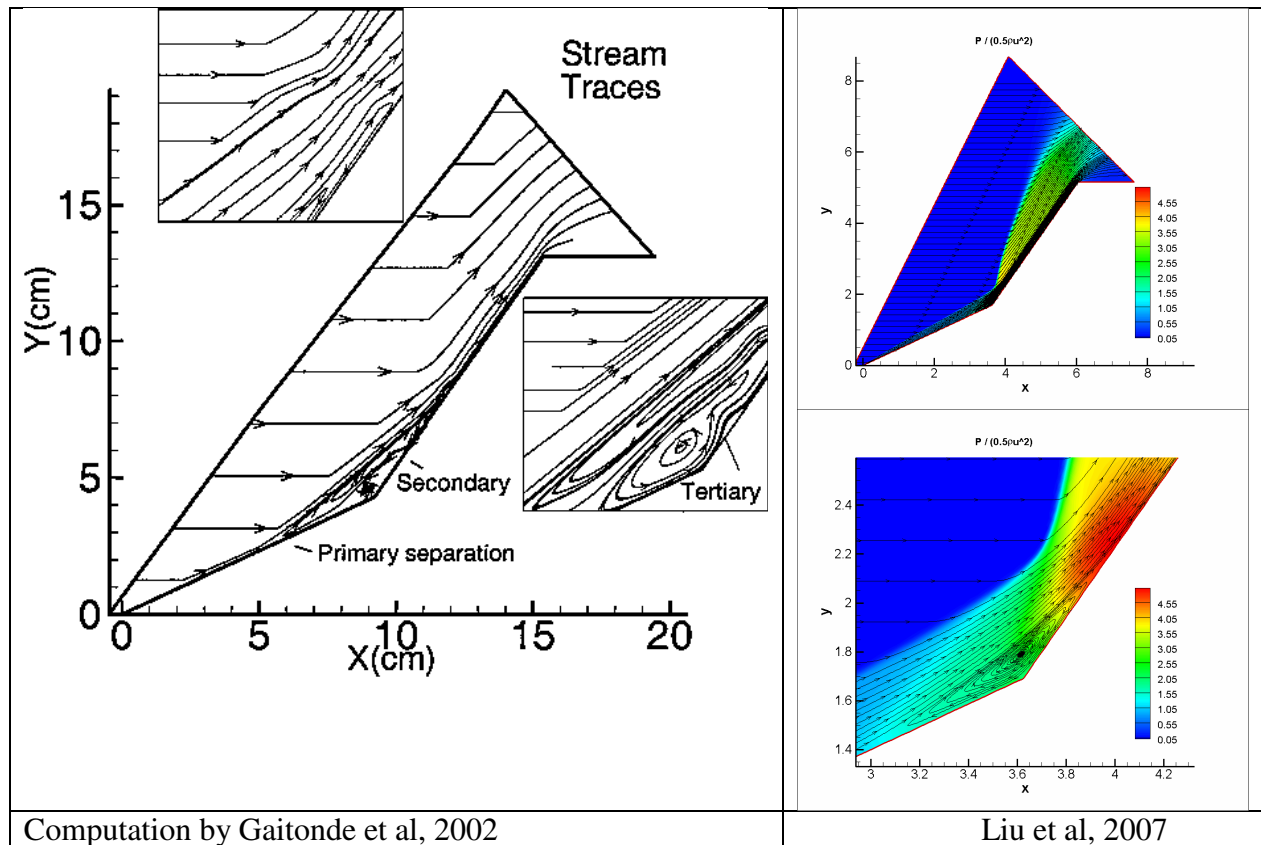


Figure 3.14 Qualitative comparison of streamline and separation bubble

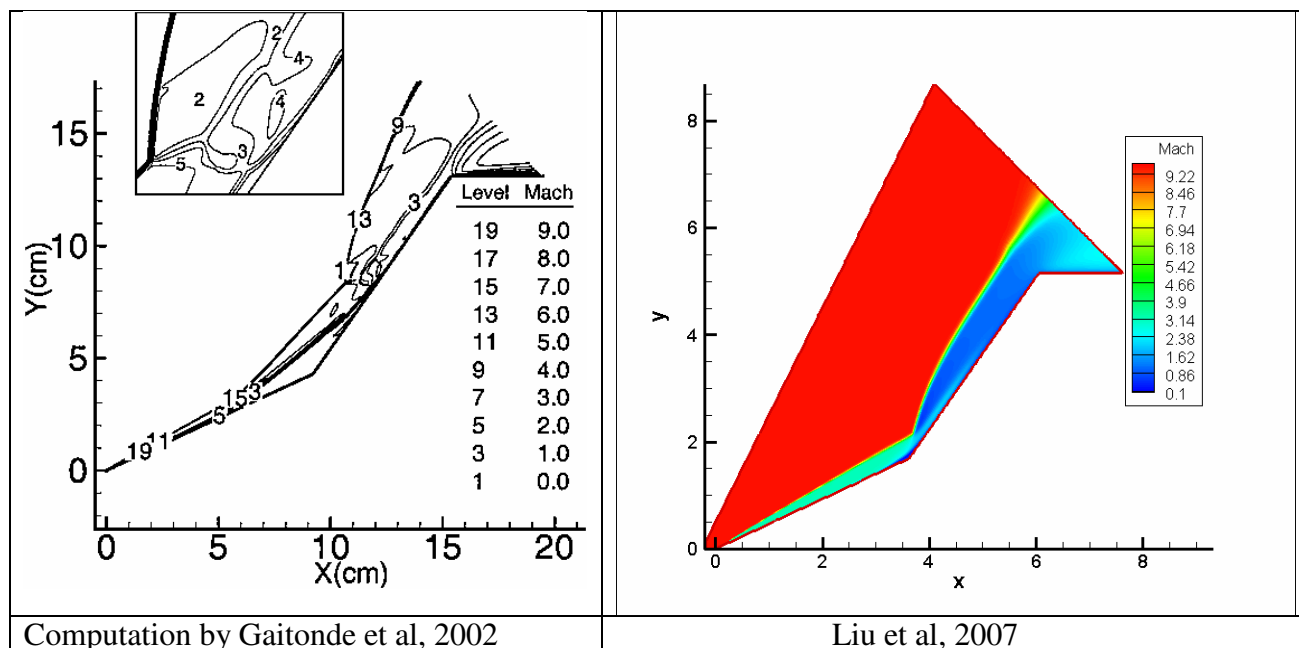


Figure 3.15 Qualitative comparison of Mach number

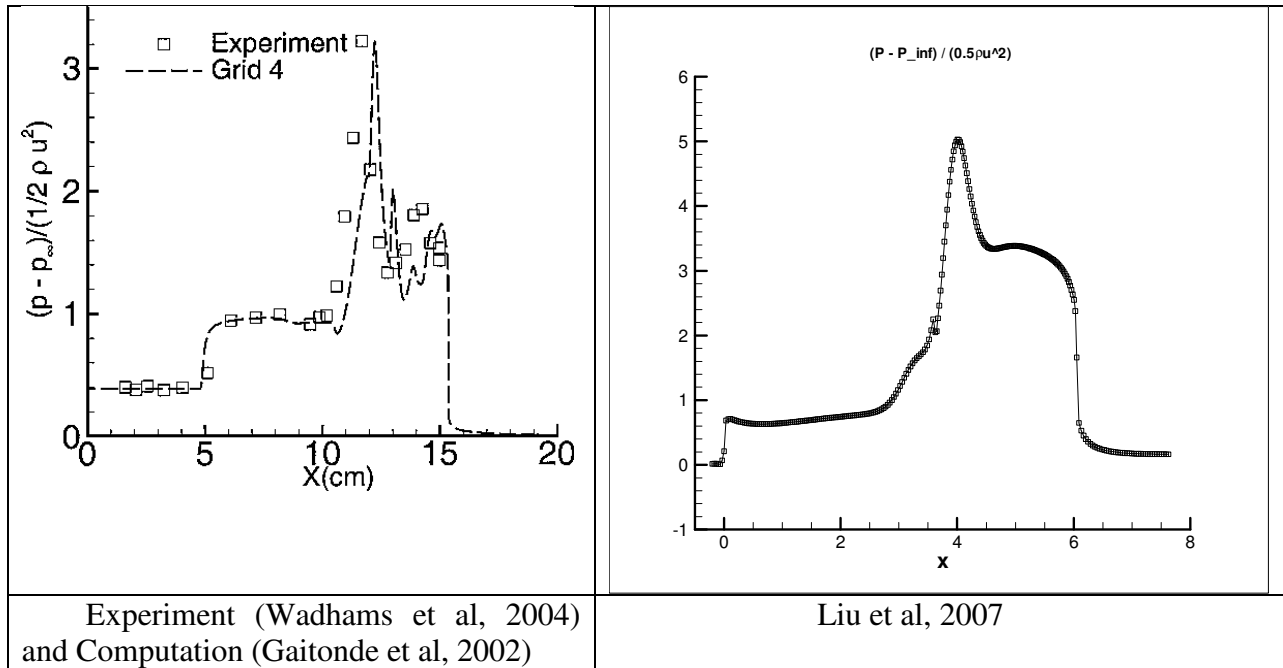


Figure 3.16 Qualitative comparison of Cp

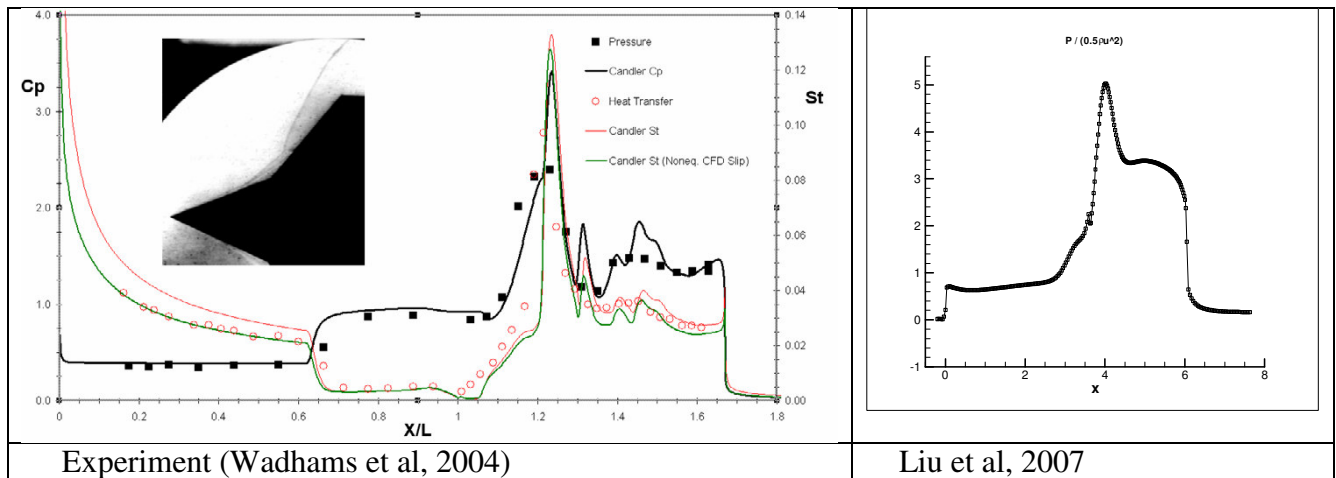


Figure 3.17 Qualitative comparison of pressure distribution

### 3.5 Preliminary results for 2-D double cone shock-boundary layer interaction at M=9.58

This work is still under development.

### 3.6 Achievements and further efforts

The following conclusions can be made based on our previous work which was supported by the current AFOSR grant ending by 12-31-07:

- 1) The original weighted compact scheme does not have enough dissipation to capture the shock without wiggles but is too dissipative in the smooth region.

- 2) The second order smart filter can help the WCS scheme remove the wiggles near the shock. However, the filter is case related and needs professional training to adjust.
- 3) The new MWCS scheme is basically a WCS scheme modified by a high order bias scheme. MWCS is in general much better in capturing both shock and small length scales than the standard 5<sup>th</sup> order WENO scheme and potentially could become an very important tool for DNS and LES of the shock and turbulent boundary layer interaction.
- 4) MWCS has sixth order of accuracy in the smooth area. For near shock grid points, weights  $\omega_0 = 1, \omega_1 = 0, \omega_2 = 0$ , MWCS still has fourth order of accuracy. Comparing with 5<sup>th</sup> order WENO which has 5<sup>th</sup> order in the smooth area and third order near the shock, MWCS is super with smaller stencils and higher order of accuracy.
- 5) MWCS is applicable for the simulation of flows containing both shock waves and small structures. This scheme uses same formulation without switching to a different scheme or using a low order filter.

During the past three years, following achievements have been made:

- 1) Developed a modified weighted compact scheme
- 2) Applied the MWCS scheme for 1-D shock tube and 1-D shock-entropy interaction and obtained very promising results
- 3) Applied the MWCS for 2-D incident shock, double angle and double cones. The incident shock results are very encouraging and the computation for double angle looks very reasonable while the double cone case is still under development.
- 4) Conducted theoretical study on the analysis of accuracy, dissipation, dispersion and weights function for both MWCS and WENO.
- 5) Developed a universal, black-box subroutine, applied it in our finite difference scheme, and delivered it to the Air Force research Lab. The subroutine can accept any discrete data as input and give a high order derivative as output, which can be used by any finite difference computation codes.

Future work will include more 2-D and 3-D shock-boundary layer interaction cases, optimization of WCS weights, modifying  $F_{bias}$  and  $\alpha(x)$ , improve the black box subroutine and dramatically reduce the computational cost required by the subroutine. In addition, we will also focus our effort on mathematical investigation of our new approaches including the accuracy, stability, dissipation, dispersion, modified governing equations, etc. The mathematical foundation is critical for new scheme development. If we do not understand well, it would not be possible to improve or optimize the new scheme.

#### 4. Acknowledgement

This work is supported by AFOSR under grant FA9550-05-1-0136 supervised by Dr. Fahroo. The author thanks Dr. Fahroo for her sponsorship. The author also thanks Dr. Gaitonde for his support through VA Summer Faculty Program.

## 4. References

- [1] Gaitonde, D, and Visbal, M, Pade-type high-order boundary filters for the Navier-Stokes equations, *AIAA Journal*, Vol. 38, No. 11, pp 2103-2112, 2000.
- [2] Gaitonde, D, Canupp, p. W., and Holden, M., Heat transfer predictions in a laminar hypersonic viscous/inviscid interaction, *Journal of thermophysics and heat transfer*, Vol. 16, No. 4, October–December 2002
- [3] Godnov, S. K., A difference scheme for numerical computation of discontinuous solution of hydrodynamic equations, *Math Sbornik*, Vol 47, 271-306 (in Russian) translated US Joint Publ. Res. Service, JPRS 7226, 1969.
- [4] Harten A, High resolution schemes for hyperbolic conservation laws, *J. of Computational Physics*, Vol 49, pp357-393, 1983.
- [5] Harten A, Engquist B, Osher, B, Charkravathy SR, Uniformly high order accurate essentially non-oscillatory schemes III, *J. of Computational Physics*, Vol 71, pp231-303, 1987.
- [6] Jiang, G. S., Shu, C. W., Efficient implementation of weighted ENO scheme. *J. Comput. Phys.*, 126, pp.202—228, 1996.
- [7] Jiang L, Shan H, Liu C, Weight Compact Scheme for Shock Capturing, *International Journal of Computational Fluid Dynamics*, 15, pp.147-155, 2001.
- [8] Lele S.K., Compact finite difference schemes with spectral-like resolution, *Journal Computational Physics*, 103, pp.16—42, 1992.
- [9] Liu, C., Xie, P., and Oliveira, M, High order modified compact scheme for high speed flow, technical report to Gaitonde at Air Force Research Lab.
- [10] Liu, D, Osher, S, Chan, T, Weighted essentially nonoscillatory schemes, *J. of Computational Physics*, V115, pp200-212, 1994
- [11] Roe, P.L., Approximate Riemann solvers, parameter vectors and difference schemes, *J. of Computational Physics*, Vol 43, pp357-372, 1981
- [12] Shu, C.W., Osher, S., Efficient implementation of essentially non-oscillatory shock-capturing scheme. *Journal of Computational Physics* 77, pp.439-471, 1988.
- [13] Shu, C. W., Osher, S., Efficient implementation of essentially non-oscillatory shock-capturing schemes II, *J. Comput. Phys.*,83, pp.32-78, 1989.
- [14] Su, Xie, Oliveira, and Liu, Error Analysis for Weighted Higher Order Compact Finite Difference Scheme, *J. of Applied Mathematical Science*, to appear.
- [15] Van Leer, B., Towards the ultimate conservative difference scheme. V. A second order sequel to Godnov's scheme, *Journal of Computational Physics*, Vol 32, pp101-136, 1979
- [16] Visbal, M. and Gaitonde, D., On the use of higher-order finite-difference schemes on curvilinear and deforming meshes' *JCP*, Vol. 181, pp155-158, 2002.
- [17] Wadhams, T. P., Holden, M. S., Summary of experimental studies for code validation in the LENS facility with recent Navier-Stokes and DSMC solutions for two- and three-dimensional separated regions in hypervelocity flows, *AIAA 2004-917 42nd AIAA Aerospace Sciences Meeting and Exhibit*, 5 - 8 January 2004, Reno, Nevada